Okinawa Institute of Science and Technology
Graduate University

Thesis submitted for the degree

Doctor of Philosophy

Supersymmetry and Nonequilibrium Quantum Dynamics

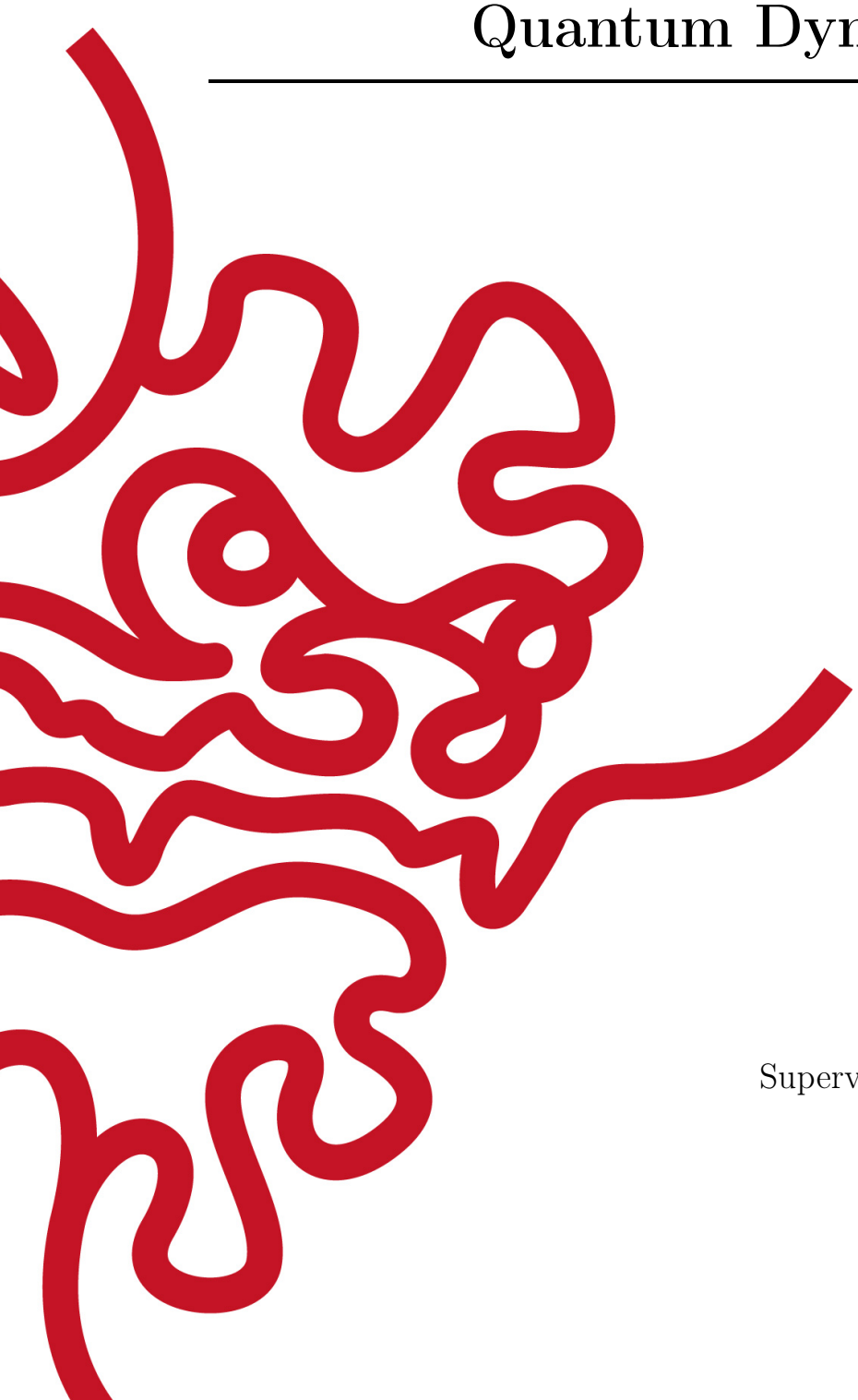

by

Christopher Campbell

Supervisor: **Prof. Thomas Busch**

December 2022

Declaration of Original and Sole Authorship

I, Christopher Campbell, declare that this thesis entitled *Supersymmetry and Nonequilibrium Quantum Dynamics* and the data presented in it are original and my own work.

I confirm that:

- No part of this work has previously been submitted for a degree at this or any other university.
- References to the work of others have been clearly acknowledged. Quotations from the work of others have been clearly indicated, and attributed to them.
- In cases where others have contributed to part of this work, such contribution has been clearly acknowledged and distinguished from my own work.
- None of this work has been previously published elsewhere, with the exception of the following:
  - The results of Chapter 4 are published as:

    Christopher Campbell, Thomás Fogarty and Thomas Busch
    Non-equilibrium many-body dynamics in supersymmetric quenching
    Phys. Rev. Research **4**, 033014 (2022) [1]

    I derived all the analytical results for the supersymmetric intertwining relationships for the survival probability and description of the phase factor as well as performed all numerical simulations and identification of transitions for the work probability distribution. I also produced the first draft of the paper to which all authors contributed to discussion, interpolation of results and final production of the material published.
  - The results of Chapter 5 are published as:

    Christopher Campbell, Jing Li, Thomas Busch and Thomás Fogarty
    Quantum control and quantum speed limits in supersymmetric potentials
    New J. Phys. **24**, 095001 (2022) [2]

    I conducted all numerical simulations and analytical results which went to the fidelity, cost, quantum speed limit and energy functional for all results.

I also derived the analytical expressions for the extended intertwining properties of the counterdiabatic driving terms specific to the infinite square well. I wrote the first draft of the paper and all other authors contributed to the discussions, interpolation of results, suggestions of improvements toward presentation of the analytical results and the final production of the material published.

- All of the above articles have been published in an open access format under the 'Creative Commons Attribution 4.0 International' license and I have permission to reprint them for the purpose of the thesis.

Date: December 2022

Signature: 

Abstract

Supersymmetry and Nonequilibrium Quantum Dynamics

In this thesis I present two studies that use ideas and concepts from supersymmetric quantum mechanics to understand and control the nonequilibrium dynamics of a quantum many-body system. The two protocols I study involve the quenching of a spin-polarized Fermi gas and the adiabatic control of single particle states during the expansion of an infinite square well over a finite time interval. In the first study, I explore the survival probability and the work probability distribution for quenches within a hierarchy of potentials created using supersymmetric factorization methods. I show that in this setting one can take advantage of the degeneracy between supersymmetric potentials in order to find simplified expressions for these quantities. I also show that many-body revivals in these systems exist and are robust even at finite temperatures. For the second study I explore a shortcut to adiabaticity (STA) based on counterdiabatic driving for the single particle states of the supersymmetric partner potentials of the infinite square. By calculating the fidelity, quantum speed limit time and the cost of driving a system, I compare the efficiency of the shortcuts between the ground state wavefunctions of three supersymmetric potentials and three wavefunctions that are isospectral to one another. The use of a supersymmetric setting allows me to distinguish between the dynamical effects stemming from the energy spectrum and from the distance between the states in Hilbert space. I also show that in the isospectral case one can develop an intertwining relationship between the counterdiabatic driving terms using the operators of their single particle Hamiltonians.

Acknowledgment

It was one shot-in-the-dark email that I sent to a man in Okinawa Japan simply because I needed advice about graduate school opportunities, I had no clue where to start. Prof. Thomas Busch. Not only well rounded in his expertise with a tenacity to explore new facets of quantum mechanics, but will support his students on both a professional and personal level that no one can reach (figuratively and quite literally). I can't thank Thomas enough for the phenomenal amount of support he not only gave me but continues to give to everyone in his unit. I'm incredibly lucky to have his support from intern to Ph.D. candidate and for pushing me and making me see this to the end all I can say is Thank You.

Equally, I could not have done this without my good friend and colleague Thomás Fogarty. When things got rocky you took me under your wing and you guided me over the past two years, helping me produce work that I can be proud of. You've seen this journey from beginning to end with me and I am so grateful for the knowledge and assistance you have given me and teaching me that Cork isn't actually all that bad. Its been great to have someone from home to lean on and to adventure outside of the office with Sawako, Kaori and Yoko, my three Okinawan mothers (In no particular order).

The same goes to all of the other members both past and present of the Quantum Systems since coming to Okinawa. Lee, for giving me sound advice as I start to look for the next step in my life. To Ayaka and James, who gave great advice during and after their studies in Okinawa, and still do even in their incredibly busy life. Sahar, for showing me how to take care of the group after you moved to the mainland, I now fear for the hat I'm going to receive in the future. Tim, it means so much to have your support with not only the work I've done in OIST but also outside and I am excited to see where the "self-pinning cult" is going to go in the future.

Over the past six years I've been lucky to be associated with so many people coming in and out of the unit and have to mention them in my journey. I have to shout out to Jing Li for her motivation of our shortcut paper. The original crew Albert, Angela, Irina, Juan, Mathias, Rashi, Yongping, Karol, Jiabao, you all motivated me to continue my work in QSU. And now we have an amazing group, Hasan, Momo, Lewis, Tai (thank you so much for you're numerical knowladge), Kritika, Seyyare, Fam, Hoshu, Eloisa, Keerty, J.C., Sarika, Hao, Wenbin, and introducing our newest post-doc Giedrius. And I need to shout out the future graduate students in the making Salome, Yuliya, Nikola and Gabriel.

Of course I couldn't have done all of this with out the support of my friends and family on both sides of the Atlantic. To my mother and father, Angela and Shawn, who supported me every step of the way and to my brother Colin who has grown up

to be an amazing engineer. Leaving Ireland to pursue my Ph.D. was always going to be a hard step and you guys kept cheering me on throughout the past 6 years. And rest assured when that when you weren't able to be there when I was having a bad day Juni was always there to pick me up and make sure that I still pushed on. Juni thank you so much for all the support from you and your family over the past five years. You always know how to keep me smiling even on your bad days.

And lastly to all the friends I've made in Okianwa, from the OIST LGBTQ+ Allies Society and the Aerial Circus group. These are no doubt the memories and experiences that will never stop talking about.

Abbreviations

SUSY	Supersymmetry
SUSY QM	Supersymmetric Quantum Mechanics
ISW	Infinite Square Well
STA	Shortcut to Adiabaticity
CD	Counterdiabatic Driving
QSL	Quantum Speed Limit
TISE	Time Independent Schrödinger Equation

If you awaken from this illusion and you understand that black implies white, self implies other, life implies death (or shall I say death implies life?), you can feel yourself – not as a stranger in the world, not as something here on probation, not as something that has arrived here by fluke - but you can begin to feel your own existence as absolutely fundamental.

-Alan Watts

To Norman J. Stuart, Frank and Phil Moran and Ann O' Flaherty. Without their support I would have never gotten to this point.

Contents

List of Figures

Introduction

Macroscopic effects in quantum mechanics, like superconductivity or the physics of semiconductors, have played a large role in the technology for several decades. More recently technology has been developed that allows one to control quantum systems made from single or few particles only. This has been partly driven by the development of ideas in quantum information and communication [4–6], which require highly accurate control of the system and high fidelities for dynamical processes. While for atoms there are many ways to control the internal degrees of freedom with great precision have been developed in the field of laser spectroscopy, the control over the external degrees of freedom only became possible recently through the emergence of flexible methods for trapping atoms in space [7]. By today many different single particle quantum systems can be prepared in their respective ground states, manipulated into a specific state, and measured with high precision. While decoherence is still an issue, especially on longer time scales, a great deal of progress is made in a continuous way.

While many of the tasks one would like to carry out in quantum information require the development of new ideas for technical realisation, they also often profit from different ways of looking or exploring them to get additional insight. In this thesis I will use ideas from supersymmetric quantum mechanics to provide an additional angle of understanding for the dynamics in ultracold quantum gases [8]. The idea behind supersymmetric quantum mechanics is that any Hamiltonian can be factorized into two operators, which can be re-combined to lead to a second, so-called supersymmetric Hamiltonian [9, 10]. Both these operators have the same eigenspectrum (apart from the lowest lying state of the first Hamiltonian) [11] and the factorisation operators connect the eigenstates of the two supersymmetric Hamiltonians. Over the years, many studies have been carried out that take advantage of this symmetry, making it a powerful tool in solving initially complex potentials into exactly solvable systems [12–14]. In recent years there has been a shift in focusing on ultracold atomic systems where supersymmetry can be applied [15–17] and in my work I will add two more studies in this spirit. In particular I will take advantage of the fact that supersymmetric operations gives access to a library of potentials which can be derived from a single common potential, in which the eigenspectra are near degenerate with the original potential. This allows one to induce a dynamics by switching between different supersymmetric potentials which is mostly driven by changes in the eigenfunctions and not the eigenspectrum, which makes it possible to identify certain effects of non-equilibrium or controlled systems that would be otherwise obscured by competing effects.

In particular I present two studies explore the two extremes of what happens to a system when it is brought out of equilibrium very quickly by means of a quench and

what happens when a system evolves over a finite period of time whilst incorporating a shortcut to adiabaticity. The first study specifically revolves around a quench of a Fermi gas between partner Hamiltonians [1]. Typically in these studies a gas is prepared using one potential which is then arbitrarily changed using a parameter of the Hamiltonian such as the interaction strength between the particles of the gas [18, 19] or a parameter which changes the strength or functional form of the external potential [20].

I show in my work that using supersymmmetric Hamiltonians to study non-equilibrium dynamics can help to understand this complex problem by isolating different aspects of the dynamics of the system. For one, the degeneracy of the energy spectrum between different Hamiltonians allows one to focus on the influence of the differences in the eigenfunctions on the dynamics. Furthermore, the existence of a hierarchy of supersymmetric Hamiltonians allows one to carry out similar studies in many different systems. This especially lends itself to studying the dynamics of an ultracold gas from the perspective of the same initial state being quenched into different, related systems. Using the infinite square well as an example, I show that certain properties of the eigenspectrum can lead to unexpected dynamics, such as the presence of high survival probabilities at finite temperatures. This is a striking feature as at finite temperature one would expect the survival probability to be destroyed due to phase mixing. I show the supersymmetric potentials offer a clear interpretation of this.

In the second project [2] I study counterdiabatic driving protocols in supersymmetric Hamiltonians [21, 22]. My central idea is that the operators that factorize the single particle Hamiltonian can also be used for the counterdiabatic term, which relies on the instantaneous, time-dependent eigenstates. This then allows to extend the intertwining relationship to the full Hamiltonian. Additionally I explore the costs of driving a shortcut and the quantum speed limit time within the hierarchy of the supersymmetric potentials associated with the infinite square well.

The thesis is laid out in two parts. The first part is meant to briefly review the background material which is central to the entire thesis, specifically the concept of optical potentials and an outline of supersymmetric quantum mechanics. In the second part each publication is highlighted as its own chapter. The chapters expand on the mathematical derivations and calculations used in the publications, whilst also highlighting the major contribution supersymmetry had in the work. The layout of the chapters are as follows:

- **Part I: Fundamental Material**
  - **Chapter 1** provides an introduction to ultracold gases and the mechanism of optical trapping.
  - **Chapter 2** introduces supersymmetry in the context of quantum mechanics. Here I describe the mathematical structure of supersymmetry, the basic concepts of factorization and the properties that connect partner Hamiltonians.
  - **Chapter 3** provides a brief description of the numerical techniques used in my work.
- **Part II: Non-equilibrium Dynamics and Quantum Control**

– **Chapter 4** highlights and expand on the calculations central to the publication

Christopher Campbell, Thomás Fogarty and Thomas Busch
Non-equilibrium many-body dynamics in supersymmetric quenching
Phys. Rev. Research **4**, 033014 (2022) [1]

– **Chapter 5** highlights the work presented in the publication

Christopher Campbell, Jing Li, Thomas Busch and Thomás Fogarty
Quantum control and quantum speed limits in supersymmetric potentials
New J. Phys. **24**, 095001 (2022) [2]

Each Chapter will have its own remarks section either addressing additional finding that are relevant to the Chapters or providing an outlook on future directions for the research. The thesis will then end on a brief summary of each publication Chapter.

Part I

Fundamental Material

Chapter 1

Ultracold Atomic Gases

The trapping of ultracold gases has been a phenomenal achievement in the last 40 years, with the highlighting achievement being the observation of Bose-Einstein condensation in 1995 [23, 24]. Producing a condensate was a pivotal moment as such systems provide a clean and controllable platform for low-energy physics to be studied. Nowadays many laboratories around the world have the means to create and study condensates under a variety of configurations [6], where the study of quantum gases goes beyond studying fundamental physics. In fact, the area has moved into a realm where the dynamics and manipulation of ultracold atom system attempts to serve applicable purposes, with atomtronics being one of the most prominent of them [6].

The central topic of this thesis revolves around how supersymmetric setups can be used to study different facets of non-equilibrium quantum dynamics. This includes quenching as well as controlled dynamics using shortcut to adiabaticity protocols. As we will see in Chapter 2, supersymmetry deals with Hamiltonians which posses near exact copies of their respective eigenspectra, which has allowed me to study evolution in different potentials but with the same spectrum. To start, however, I will first introduce the idea of optical potentials and comment on recent developments that allow to large flexibility in the shapes that can be achieved. I will then discuss the ultracold Fermi gas and point out why it is a versatile gas to study both theoretically and in experiments. Finally, I will comment on lower dimensions, from an experimental and theoretical point as well.

1.1 Trapping an Ultracold gas

The most common instrument used to trap a gas of ultracold atoms is the magneto-optical Trap (MOT) [25]. This type of trapping uses a combination of spatially varying magnetic fields and counter-propagating laser beams in order to first slow down a gas of atoms, and then contain the gas in order to prevent it from escaping. The underlying mechanism for this process is known as Doppler cooling [26, 27], in which through a series of photon absorption and emission processes, the gas of atoms undergoes a constant transfer of momentum confining them to a small region of space [28]. In the following I will provide a brief summary of the process of the cooling an atomic gas, leading up to the description of the optical potential.

1.1.1 Laser Cooling

In order for an atom to absorb a photon the frequency of light required has to correspond to the energy needed for an electron to transition from one state to another in the atom. However, due to Doppler broadening, i.e. when the motion of the atom is taken into consideration, these frequencies can broaden. In the atoms frame of reference, the frequency observed is a Doppler-shifted frequency. Any absorption/emission process imparts momentum kicks onto the atom, and cooling via laser absorption and emission can therefore only reach a lower limit, known as the recoil temperature.

The process of cooling an atom can be understood by studying the interactions between light and matter. Take for example a situation where a neutral atom is moving towards a laser source pointed in the opposite direction of the atoms path. If the light is red detuned to the resonant frequency of the atom, a photon will be absorbed imparting a transfer of momentum in the direction opposite of the atoms velocity. This slows the atom. When the photon is emitted again, a recoil is imparted on the atom, however the direction of this recoil is random and therefore averages out over many such processes. Therefore, using three sets of counter-propagating lasers beams in all orthogonal spatial directions allows to reduces the velocity of the atoms over time and thereby the temperature of the gas, $T = \frac{1}{2k_B} m v^2$. However, this kind of cooling is limited in the temperature it can achieve and one needs to employ advanced methods such as polarization gradient or Sisyphus cooling to reach the ultimate recoil temperature $T = \frac{(\hbar k)^2}{m k_B}$. Here k is the wavevector of the light used to cool the atom.

To cool a gas below the recoil limit, other cooling techniques need to be employed, in particular evaporative cooling. This technique relies on removing the hottest atoms from the trap and relying on subsequent scattering processes within the gas to rethermalise the sample at a lower temperature. While this technique has worked exceptionally well for bosons, it is slightly more complicated to drive a Fermi gas into the degenerate regime, as spin-polarised fermions do not scatter at low temperatures. Experimentally it was therefore necessary to introduce a second fermionic component or an additional Bose-Einstein condensate into the trap to facilitate sympathetic cooling [29, 30].

1.1.2 Optical Potentials

So far we introduced how to cool a gas of atoms but have not addressed how to contain the gas. Since the atoms are constantly undergoing a momentum transfer due to photon absorption and emission, which means that they are prone to being kicked out of the space they occupy, an external trapping potential needs to be constructed as well. Optical potentials provide a versatile platform for the confinement of atoms once their velocity is sufficiently low [31].

The optical field of a laser can be written as

$$\vec{E}(x,t) = E_0(x) e^{-i\omega t} + E_0(x) e^{i\omega t} \,, \tag{1.1}$$

where ω is the frequency of the electric field and E_0 is the amplitude [32]. Since the wavelength of the laser is much larger than the size of the atom, the dipole approxi-

mation can be used to describe the interaction between the field and the atom, namely

$$V(x,t) = \vec{d} \cdot \vec{E} \, . \tag{1.2}$$

The interaction induces a dipole polarization causing the atom to oscillate at the same frequency as the field, where the average dipole moment is given by

$$\langle d \rangle = \alpha(\omega)(\vec{E}(x,t)), \tag{1.3}$$

and where α is the polarizability of the atom. This dipole interaction induces an energy shift, the effect of which can be described using an effective potential

$$U(x) = \frac{1}{2}\alpha(\omega)\overline{\vec{E}^2(x,t)}, \tag{1.4}$$

where the time average of the electric field is considered.

The effective potential in Eq. (1.4) gives rise to the force acting on the atomic cloud, depending on the distribution of the radiation intensity and frequency of the laser. The polarizability depends on the detuning $\delta = \omega - \omega_R$, where ω_R is the resonance frequency of the atom. For a positive detuning (blue detuning) the laser field acts repulsively on the atom pushing it towards lower field strengths. On the other hand negative detuning (red detuning) attracts the atoms to areas of higher field strengths, which means that both of these can be used for optical trapping. This type of confinement offers a wide range of versatility in experiments, as optical potentials can be easily manipulated in order to create unique geometries for a wide range of studies [7, 33, 34]. In the next section I will provide an example of the resulting potential that arises from the counter-propagating beams, namely the optical lattice [35].

1.1.3 Optical lattice and low dimensional gases

Having counter-propagating laser beams leads to interference and to the formation of a standing wave. This can be interpreted as a periodic potential for the atoms and is therefore referred to as an optical lattice [36]. To start consider two laser beams counter-propagating along the x-direction with electric fields of the form $\mathbf{E}(x,t) = E_0(t)e^{\pm ik_x x}$. Here the direction of propagation is given by the positive or negative sign, E_0 is the amplitude of the electric field and k_x is the wavevector. Through constructive and destructive interference a sinusoidal standing wave is created, such that the potential is proportional to $V_x \propto \cos^2(k_x x)$. Doing the same in the y and z directions with laser beams of different polarisation or slightly different wavelength to avoid interference in different spatial directions, a full three dimensional lattice can be formed (see Fig. 1.1 b)

$$V(x,y,z) = V_x \cos^2(k_x x) + V_y \cos^2(k_y y) + V_z \cos^2(k_z z) \, . \tag{1.5}$$

A potential of this nature creates an array of periodic wells formed by the nodes or anti-nodes of the counter-propagating lasers, depending on the detuning. As mentioned previously red-detuned light attracts atoms to areas of higher electric fields and the atoms will align accordingly to the maxima of the lattice. Blue-detuned light, on the other hand, will attract atoms to areas of minimum intensity.

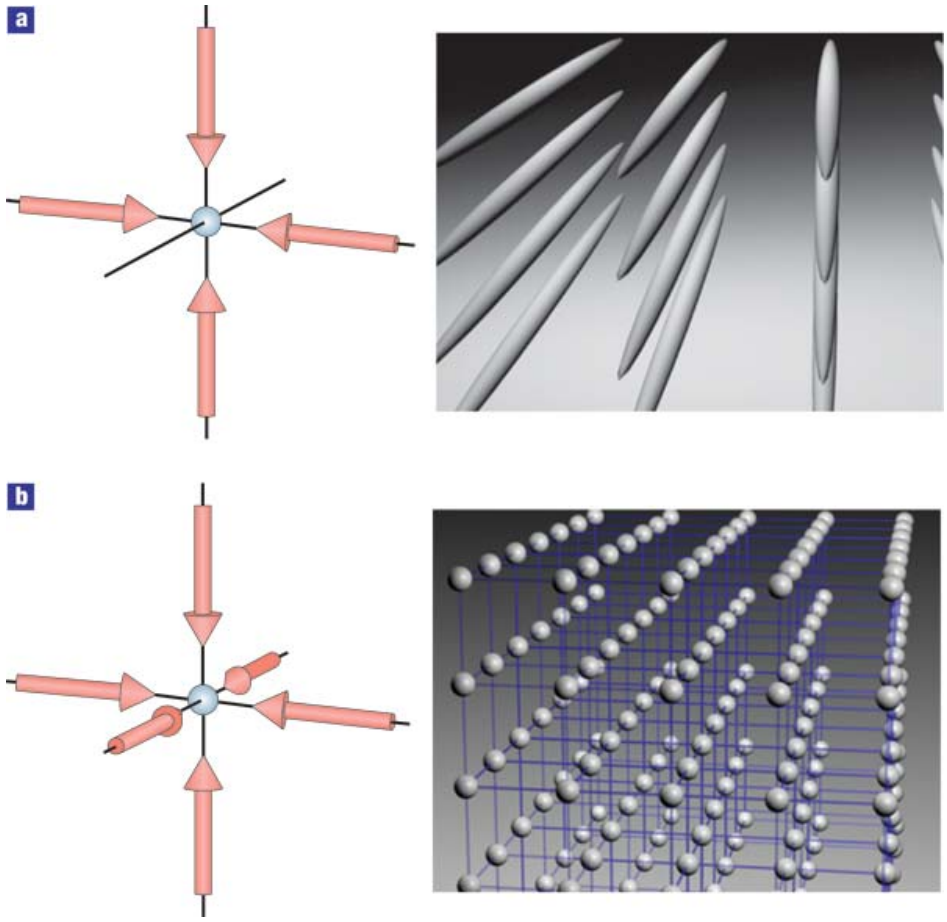

Figure 1.1: Illustration of the different geometries of a) an optical lattice of elongated potentials and b) a three dimensional lattice of spherical potentials. Taken from [3].

A further perk of interfering laser beams is that by only using lattice beams in certain directions and not in others, one can tune the dimensionality for an atomic gas. For example, an effectively one-dimensional potential can be created by only applying counter-propagating laser beams in two directions, such that the atoms are tightly trapped in these, but can easily move in the remaining one. The effective transverse trapping frequencies in such a system are much larger than the axial one ($\omega_x \ll \omega_\perp$) and the dynamics in the transversal direction is suppressed (if no energy scale exceeds the transversal harmonic oscillator energy, $k_b T \ll \hbar\omega_\perp - \mu$). In experiments this results in a periodic array of elongated cigar shaped tubes, see Fig. 1.1 a.

While simulating physics in lower dimensions is usually numerically easier, it can also be drastically different from what one would find in higher dimensions. This is mostly due to the fact that in lower dimensions correlations are usually much stronger, which can lead to new phases of matter with unique and interesting properties [37].

1.2 Experiments in Ultracold gases

The first successful creation of a Bose-Einstein condensate was in a 3D trap and the system consisted of about 10^6 atoms [23, 24]. Efforts to realise systems in reduced the dimensionality culminated in the realisation of a one-dimensional Tonks-Girardeau gas in 2004 [38, 39]. Parallel to these developments the first ultracold Fermi gases were being created [29, 30, 40]. The differences in their cooling and stability provided advantages and disadvantages. While the properties of bosonic gases were to a large degree determined by the interactions between the particles, in spin-polarised ultracold Fermi gases s-wave scattering processes were absent due to the Pauli exclusion principle. This allows these systems to be described using an ideal gas formalism. However, interactions in Fermi gases could be observed in non-spin polarised systems, which lead to the observation of superfluidity of fermionic pairs [41] as well as the exploration into the BEC-BCS crossover region [42, 43].

Undoubtedly, the most interesting property of a fermionic system is its quantum statistics [44]. In Chapters 4 and 5 I will describe the use of a spin-polarized Fermi gas in order to study the non-equilibrium many-body dynamics induced by a quench and controlled many-body dynamics through a shortcut to adiabaticity. At zero temperature the spin-polarized Fermi gas occupies the lowest lying eigenstates and forms a Fermi sea, and the presence of the Pauli principle has significant implications for the allowed dynamics.

1.3 Advances in Atom Trapping

The ability to trap a gas in a variety of different geometries is one of the keys for being able to control the center of mass mode with large flexibility [6]. Over the recent two decades the precision with which neutral atoms can be trapped has moved from being able to control the center of mass of atomic clouds to doing the same for single atoms. New methods for trapping atoms have emerged in recent years that rely on higher order mode beams, holographic setups, or time-averaging methods. These allow for the creation of non-trivial potentials such as ring traps when using Laguerre beams [45], which can also be used to create ring optical lattices [46–48].

More recently optical tweezers have become promising tools, which are made from highly focused lasers that can trap and move single atoms in their focus with large precision [17, 49]. This allows to create atomic systems in an atom-by-atom assembly way and therefore offer an unprecedented amount of flexibility. At the same time experimental progress is made using so-called painted potentials, where averaging the potential from a fast moving laser beam allows to create a variety of geometries and configurations in three dimensions [7, 50, 51]. This is done by use of spatial light modulators (SLMs) with holography in order to shape a potential to a desired structure. Combined with optical tweezers, atoms can be loaded in these painted potentials creating complex arrays of optical lattices. Details on how to shape such light structures have been summarised in several excellent reviews [52, 53], and most recently techniques from supersymmertric quantum mechanics have been used as a means to filter eigenstates of specific energy levels in order to construct potentials where the spectral

energies are all prime numbers [54]. For my work in particular one can note that these techniques make it possible to create also the specific shapes of the supersymmetric partner potentials required.

Chapter 2

Supersymmetric Quantum Mechanics

In this Chapter I will provide a detailed summary of the mathematical structure and properties of supersymmetric quantum mechanics used in the work presented. Originally derived as a method for connecting fermionic and bosonic Hilbert spaces in high-energy physics, supersymmetry introduces a general closed Lie algebra that connects the Hilbert spaces of two Hamiltonians. In both systems, the eigenspectra remain the same whilst dynamical comparisons between the Hamiltonians can be made from the overlap of the wavefunctions alone. In this chapter I will introduce the formal consequences that arise from the factorization of a Hamiltonian into a set of operators which allow to create supersymmetric partner Hamiltonians. In particular I will detail how these operators transform eigenfunctions and lead to intertwining properties of Hamiltonians. I will show that this method is recursive and, in fact, a hierarchy of Hamiltonians can be derived from this factorization method. Finally I will present a case example by factorizing the Hamiltonian of the infinite square well, and explicitly build a set of supersymmetric partner potentials that will be used throughout the thesis.

2.1 Factorization and Hamiltonian Construction

The factorization of a Hamiltonian is a technique that was initially introduced by Dirac [55]. It was later expanded on by Schrödinger, who applied the factorization method to a number of examples including the Couloumb potential [9], and by Infeld, who used it for solving *some* eigenvalue problems [56] with applications of these explored by Hull [10, 57]. Further progress was made by Sukumar, who showed that the method could be applied to any one-dimensional potential as long as there is a normalizable eigenstate [58]. The basic ingredient of this method are two operators, which mirror those of the standard creation and annihilation operators used in harmonic oscillators. However, rather than moving states up and down the eigenspectrum, the transformation occurs laterally into adjacent Hilbert spaces of the supersymmetric Hamiltonians of the same family.

Let me start by introducing the algebra central to supersymmetry [8]. In a manner similar to the creation and annihilation operators of the harmonic oscillator, a single-particle Hamiltonian with a normalizable ground state wavefunction can be factorized

into a set of two adjoint operators, which throughout this thesis will be written as A and $A^\dagger$, as

$$H = -\frac{\hbar^2}{2m}\frac{d^2}{dx^2} + V(x) = A^\dagger A. \tag{2.1}$$

These operators, the annihilation and creation operators respectively, can be written as

$$A = \frac{\hbar}{\sqrt{2m}}\frac{d}{dx} + \mathcal{W}(x), \tag{2.2}$$

$$A^\dagger = -\frac{\hbar}{\sqrt{2m}}\frac{d}{dx} + \mathcal{W}(x), \tag{2.3}$$

where $\mathcal{W}(x)$ is a function commonly known as the superpotential. It is directly related to the potential in the Hamiltonian (2.1) as

$$V(x) = \mathcal{W}(x)^2 - \frac{\hbar}{\sqrt{2m}}\frac{\mathcal{W}'(x)}{\sqrt{2}}\ , \tag{2.4}$$

where $\mathcal{W}'(x)$ is the spatial derivative of the superpotential. The superpotential can be calculated from the ground state wavefunction of the first Hamiltonian, when shifting its energy to zero to ensure that the following annihilation condition is met

$$A\ \psi_0 = 0\ . \tag{2.5}$$

The superpotential can then be simply found algebraically from

$$\mathcal{W}(x) = -\frac{\hbar}{\sqrt{2m}}\frac{\psi_0'}{\psi_0}\ , \tag{2.6}$$

and, in a situation where the superpotential is known, the ground state wavefunction can be found with some simple rearrangement from

$$\psi_0 = N \exp\left(\int_0^x \frac{-\sqrt{2m}}{\hbar}\mathcal{W}(y')dy'\right)\ , \tag{2.7}$$

where N is a normalization constant. With the knowledge of this superpotential one can now construct a partner Hamiltonian that is supersymmetric to the first one. This is achieved by simply reversing the order of factorization operators, so that in terms of the superpotential we have

$$H^{(1)} = A^\dagger A = -\frac{\hbar^2}{2m}\frac{d^2}{dx^2} + V^{(1)}(x) = -\frac{\hbar^2}{2m}\frac{d^2}{dx^2} + \mathcal{W}(x)^2 - \frac{\hbar}{\sqrt{2m}}\frac{\mathcal{W}(x)'}{\sqrt{2}}, \tag{2.8}$$

$$H^{(2)} = AA^\dagger = -\frac{\hbar^2}{2m}\frac{d^2}{dx^2} + V^{(2)}(x) = -\frac{\hbar^2}{2m}\frac{d^2}{dx^2} + \mathcal{W}(x)^2 + \frac{\hbar}{\sqrt{2m}}\frac{\mathcal{W}(x)'}{\sqrt{2}}\ , \tag{2.9}$$

where we have added superscript indices to the Hamiltonians to indicate that they are partners. As it can be seen above, the two Hamiltonians are both determined by the common superpotential. In the next section I will discuss a number of helpful relations

that can be inferred by using the factorization method.

2.2 Properties of SUSY Partner Potentials

Supersymmetric operators and the Hamiltonians created from them possess a number of unique properties. In the previous section I referred to the operators A and $A^\dagger$ as creation and annihilation operators. This is because similar to the ladder operators in the harmonic oscillator, the SUSY operators are applied to destroy or create a node in the state they are applied to [12]. The distinction between the two sets of operators however is that the ladder operators act in order to increase or decrease the energy of an eigenstate whereas in supersymmetry the energy remains the same, however the new state is an eigenstate of the partner potential.

2.2.1 Degeneracy and Wavefunction Transformations

Let us consider a pair of partner Hamiltonians $H^{(1)}$ and $H^{(2)}$ constructed using the operators A and $A^\dagger$. The Schrödinger equation for an eigenstate of $\psi_n^{(1)}$ of $H^{(1)}$ is written as

$$H^{(1)}\psi_n^{(1)} = A^\dagger A\psi_n^{(1)} = E_n^{(1)}\psi_n^{(1)} \ , \tag{2.10}$$

where we assume that the energy of the ground state is $E_0^{(1)} = 0$. If this is not the case, then the potential would require an energy shift so that the annihilation condition of the ground state $\psi_0^{(1)}$ holds true. Despite $H^{(2)}$ being constructed using the same operators, the state $\psi_n^{(1)}$ is not an eigenfunction of this Hamiltonian. However by using the operator A on the wavefunction one can write

$$H^{(2)}(A\psi_n^{(1)}) = AA^\dagger A\psi_n^{(1)} = AH^{(1)}\psi_n^{(1)} = E_n^{(1)}(A\psi_n^{(1)}) \ , \tag{2.11}$$

and similarly for $H^{(1)}$

$$H^{(1)}(A^\dagger\psi_n^{(2)}) = A^\dagger AA^\dagger\psi_n^{(2)} = A^\dagger H^{(2)}\psi_n^{(2)} = E_n^{(2)}(A^\dagger\psi_n^{(2)}) \ . \tag{2.12}$$

One can see that the operators facilitate a transformation of the eigenfunctions, converting them to eigenfunctions of the partner Hamiltonian. However, this transformation conserves the eigenvalue which means that the spectra of $H^{(1)}$ and $H^{(2)}$ are degenerate with the exception of the ground state in $H^{(1)}$.

We now need to describe these transformations between Hilbert spaces. The creation and annihilation operators act to destroy and create a node in the wavefunction, which also explains why the annihilation of the ground state of $H^{(1)}$ leads to a vacuum state, see Eq. (2.5). Since these operators mirror the harmonic oscillator ladder operators we can use a similar derivation to normalize the transformation [59]. Starting with the factorized form of the Hamiltonian

$$\langle\psi_n^{(1)}|A^\dagger A|\psi_n^{(1)}\rangle = \langle\psi_{n-1}^{(2)}|\psi_{n-1}^{(2)}\rangle c_n^* c_n \ , \tag{2.13}$$

where $c_n^{(*)}$ is a normalization constant generated from the operator transformations, we

find using Eq. (2.10)

$$E_n^{(1)} = |c_n|^2. \tag{2.14}$$

With these considerations the final transformation can then be written as

$$\begin{aligned} A|\psi_n^{(1)}\rangle &= c_n|\psi_{n-1}^{(2)}\rangle, \\ A|\psi_n^{(1)}\rangle &= \sqrt{E_n^{(1)}}|\psi_{n-1}^{(2)}\rangle, \\ \frac{A|\psi_n^{(1)}\rangle}{\sqrt{E_n^{(1)}}} &= |\psi_{n-1}^{(2)}\rangle \ . \end{aligned} \tag{2.15}$$

For a transformation using the creation operators the same procedure is used and can be generalized as

$$\frac{A^\dagger|\psi_{n-1}^{(2)}\rangle}{\sqrt{E_{n-1}^{(2)}}} = |\psi_n^{(1)}\rangle \ . \tag{2.16}$$

2.2.2 Intertwining Relationships

The degeneracy of the two eigenspectra also introduces an interesting property of SUSY, namely intertwining relationships. Due to the construction of these Hamiltonians, annihilation and creation operators can be used to create a relationship between the two Hilbert spaces. The most straightforward demonstration of this is to apply the annihilation operator to each Hamiltonian, giving

$$H^{(2)}A = AA^\dagger A = AH^{(1)} \ . \tag{2.17}$$

As a consequence, the respective time evolution operators also possess an intertwining property. For example, the time-evolution operator for $H^{(2)}$ is

$$U^{(2)}(t) = e^{-\frac{i}{\hbar}H^{(2)}t}, \tag{2.18}$$

which can be expanded using a Taylor series of the exponential term as

$$e^{-\frac{i}{\hbar}H^{(2)}t} = \sum_{k=0}^{\infty} \frac{1}{k!}\left(-\frac{i}{\hbar}H^{(2)}t\right)^k \ . \tag{2.19}$$

Applying the annihilation operator to the form from the left, and using the identity in Eq (2.17), an intertwining relationship for the time-evolution operators is given by

$$AU^{(1)}(t) = U^{(2)}(t)A. \tag{2.20}$$

It is interesting to note that this corresponds to a transition from intertwining properties being time independent to being time dependent. This allows for the dynamics of a wavefunction to be measured amongst two Hilbert spaces. In particular, this is an important result to identify if an evolving system possesses supersymmetric properties [16].

2.3 Higher order potentials

So far in our derivations of partner Hamiltonians we did start with a given Hamiltonian $H^{(1)}$ with a ground state ψ_0 and constructed a second Hamiltonian $H^{(2)}$ by finding the superpotential $\mathcal{W}(x)$. If the second Hamiltonian also contains a normalizable ground state wavefunction, then the factorization process can be applied recursively, and a hierarchical family of supersymmetric Hamiltonians can be constructed [58]. For this one needs to create a second set of SUSY operators, defined by $A^{(2)}\psi_0^{(2)} = 0$. This then, in turn, allows to create another partner Hamiltonian by flipping the operators $A^{(2)}$. In fact, this process can be repeated for the next Hamiltonian, $H^{(3)}$, and one can obtain a hierarchy of Hamiltonians as

$$\begin{aligned} H^{(2)} = A^{(1)}A^{(1)\dagger} =& A^{(2)\dagger}A^{(2)} \\ H^{(3)} =& A^{(2)}A^{(2)\dagger} = A^{(3)\dagger}A^{(3)} \\ H^{(4)} =& A^{(3)}A^{(3)\dagger} = A^{(4)\dagger}A^{(4)} \ \ldots . \end{aligned} \tag{2.21}$$

It is important to clarify that while a family of Hamiltonians can be created using this process, only pairs of Hamiltonians using the same SUSY operators can be considered partner Hamiltonians. Partner Hamiltonians possess intertwining properties which are connected to their common superpotential.

For Hamiltonians in the same hierarchy of supersymmetric Hamiltonians, but which do not possess the same SUSY operators (i.e. which are not adjacent) the procedure of transforming the eigenfunction between them is relatively straight forward. This time we allow for the energy of the ground state to be finite, i.e. $E_1^{(\alpha)} > 0$ at all orders. The first operator transformation transforms an eigenfunction as

$$\frac{A^{(1)}|\psi_n^{(1)}\rangle}{\sqrt{\Delta E_n^{(1)}}} = |\psi_{n-1}^{(2)}\rangle \ , \tag{2.22}$$

where the difference in energy, $\Delta E_n^{(1)}$ is between the transformed eigenstate and the ground state of the original potential $\Delta E_n^{(1)} = E_n^{(1)} - E_1^{(1)}$. This uses operators specific to $H^{(1)}$ and $H^{(2)}$, as per Eq. (2.21). Between the Hamiltonians $H^{(2)}$ and $H^{(3)}$, a different set of operators are required, $A^{(2)}$ and $A^{(2)\dagger}$, and to transform to the next higher order requires another transformation using this set of operators

$$\frac{A^{(2)}|\psi_{n-1}^{(2)}\rangle}{\sqrt{\Delta E_{n-1}^{(2)}}} = |\psi_{n-2}^{(3)}\rangle \ , \tag{2.23}$$

where $\Delta E_{n-1}^{(2)} = E_{n-1}^{(2)} - E_1^{(2)}$. In general, to transform the m-th eigenstate of the original potential to the ground state of the m-th order supersymmetric potential, the

transformation can be written as

$$\left(\prod_{n=1}^{m}\frac{A^{(n)}}{\sqrt{\Delta E_{m-n+1}^{(n)}}}\right)|\psi_m^{(1)}\rangle = |\psi_1^{(m)}\rangle\ . \tag{2.24}$$

2.4 Example: SUSY treatment of Infinite Square Well

To better introduce the system that I use for the work presented in my publications, I discuss the supersymmetric properties of the infinite square well (ISW) in the following [58, 60].

I consider a one-dimensional infinite box of length L that is centered around the origin

$$V^{(1)}(x) = \begin{cases}\infty, & \text{if } |x| > \frac{L}{2}\ ,\\ 0, & \text{if } |x| < \frac{L}{2}\ .\end{cases} \tag{2.25}$$

The single particle eigenstates can be written as

$$\psi_n^{(1)}(x) = \sqrt{\frac{2}{L}}U_{n-1}\left(\sin\left(\frac{x\pi}{L}\right)\right)\cos\left(\frac{x\pi}{L}\right), \tag{2.26}$$

where $n = 1, 2, 3....$ The functions $U_{n-1}(\sin\left(\frac{x\pi}{L}\right))$ are the Chebychev polynomials of the second kind and the form of these polynomials can be found in many books [61, 62]. Taking the ground state $\psi_1^{(1)} = \sqrt{\frac{2}{L}}\cos\left(\frac{x\pi}{L}\right)$ one can use Eq. (2.6) to find the superpotential as

$$\mathcal{W}^{(1)} = \frac{\pi\hbar}{\sqrt{2m}L}\tan\left(\frac{x\pi}{L}\right)\ , \tag{2.27}$$

which directly allows to calculate the partner potential of $V^{(1)}$ to be

$$V^{(2)}(x) = \frac{\hbar^2\pi^2}{2mL^2}\left(\sec^2\left(\frac{x\pi}{L}\right) + \tan^2\left(\frac{\pi x}{L}\right)\right)\ . \tag{2.28}$$

For the infinite square well this can be generalised and an analytical form for all higher order superpotentials can be found as

$$\mathcal{W}^{(\alpha)} = \alpha\frac{\hbar\pi}{\sqrt{2m}L}\tan\left(\frac{x\pi}{L}\right)\ . \tag{2.29}$$

The functional forms of the first four supersymmetric potentials together with the spectrum and the eigenfunctions are shown in Fig. 2.1. In fact, an analytical expression for the ground and first excited states of the full hierarchy of the supersymmetric

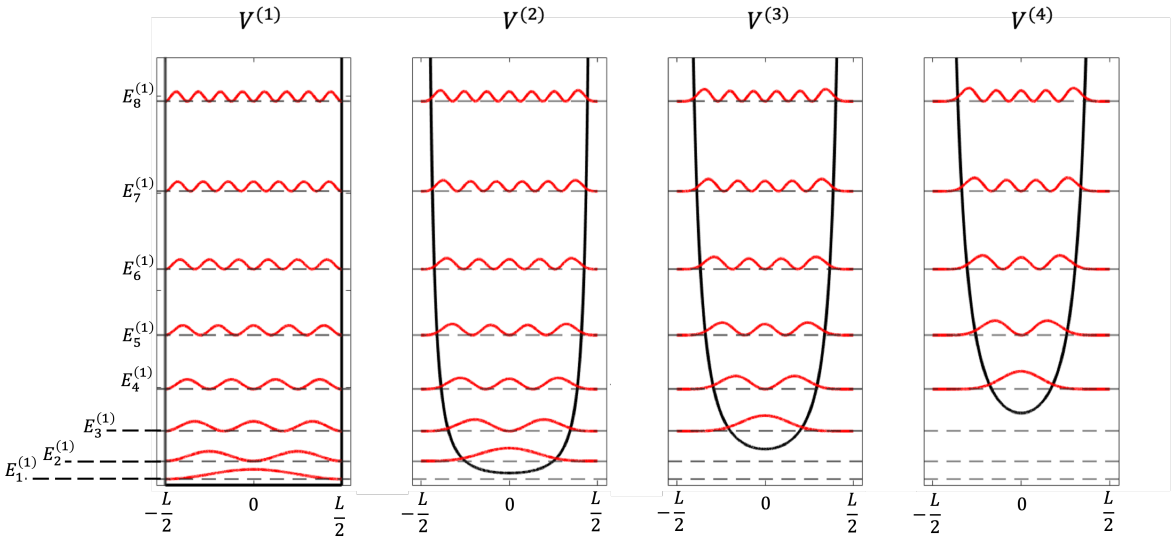

Figure 2.1: The infinite square well potential and the next three higher order supersymmetric potentials. The spectra and the eigenfunctions are also shown.

Hamiltonians of the infinite box can be found as [60]

$$\psi_1^{(\alpha)} = \frac{1}{\sqrt{L(t)}} \left[\frac{\sqrt{\pi}\Gamma(\alpha+1)}{\Gamma(\alpha+\frac{1}{2})}\right]^{\frac{1}{2}} \cos\left(\frac{x\pi}{L(t)}\right)^{\alpha}, \tag{2.30}$$

$$\psi_2^{(\alpha)} = \frac{1}{\sqrt{L(t)}} \left[\frac{2\sqrt{\pi}\Gamma(\alpha+2)}{\Gamma(\alpha+\frac{1}{2})}\right]^{\frac{1}{2}} \sin\left(\frac{x\pi}{L(t)}\right) \cos\left(\frac{x\pi}{L(t)}\right)^{\alpha}. \tag{2.31}$$

I will use these general formulas later in the analytical derivation of different quantities.

2.5 Supersymmetry in Quantum Systems

Recently SUSY QM has made its way into a number of theoretical models and systems for a variety of reasons. A popular class of potentials to study the influence of SUSY are hyperbolic functions such as the modified Pöschl–Teller potential [63]. These potentials, along with other potentials such as Couloumb and 3D harmonic oscillator potentials, possess relationships with one another [64]. These potentials lead to advances in physics and chemistry for providing models of the energy spectra of molecules for example [14]. They are also great examples to demonstrate the properties of supersymmetry, for example by showing that the hierarchy related to the sech potential possesses reflectionless properties [65]. Other Hamiltonians have in recent years been identified as possessing supersymmetric partners, such as the Jaynes-Cummings model [66], which can be used to demonstrate the construction of maximally entangled states [67, 68].

In a more application driven setting, the degeneracy between the different potentials has been suggested to play a useful role in the engineering of specific quantum systems. For example, the emergence of optical tweezers provides a high level of con-

trol over single atoms, and the preparation of ground states through tunneling between supersymmetric partner potentials has been suggested [17]. Analogies between the Schrödinger equation and the Helmholtz equation have also allowed analogies to be drawn in quantum optics [69–71]. The analogies of the Helmholtz equation leads to the continuous transformation and filtering of the modes in waveguides as well as mode division multiplexing [72, 73]. Finally with the increased precision of spatial light modulators and their high level of control in the construction of different potentials one can imagine that, in the not too far future, any potential shape can be experimentally realised [54].

Quantum dynamics in supersymmetric systems, on the other hand, has not received much attention in the community by today. Some studies have shown how quantum systems can be classified as supersymmetric using out-of-time-order correlations and wavefunction overlaps [16, 74]. Conversely, other works have implemented a Darboux transformation in order to find time-dependent solutions to the Schrödinger equation [75–78]. In this thesis I will to present two examples of physics where a supersymmetric setting is helpful. First, I extend the ideas of Lahrz *et al.* [16] by exploiting the intertwining relationship of the time-evolution operators in a quench setting. Second, I apply time-dependent supersymmetric operators to the dynamics of a shortcut to adiabaticity (STA). Supersymmetry in conjunction with dynamical invariants has been studied before in order to extend the SUSY factorization procedure [21, 22], however I show that intertwining relationships between adjacent potentials also allows to relate values such as the cost to drive a system to perfect fidelity between potentials of different order.

Chapter 3

Quantum Dynamics and Numerical Methods

In this Chapter I will briefly discuss the numerical methods used in the work presented in the thesis. To motivate this I will start by describing how finite difference methods are formulated using the Schrödinger equation. From there I will start with the example of exact diagonalization to show how one can implement such a scheme to find the stationary states and eigenspectrum of a Hamiltonian. After that I will turn my attention to the dynamics of a quantum state and show how modifications to different schemes can mitigate errors incurred in simulations.

3.1 Finite Difference Methods

Finite difference methods are numerical techniques that allow for the approximation of derivatives using discretized steps over space and time. This is a technique that is commonly used to study partial differential equations such as the Schrödinger equation and other ordinary differential equations [79]. In our case the function to discretize is the wavefunction and for its time evolution in the Schrödigner equation the time derivative can be broken up into a forward or backwards difference method respectively such that

$$\frac{\psi^{(k+1)} - \psi^{(k)}}{\Delta t} \approx \frac{\partial \psi^{(k)}}{\partial t}, \tag{3.1}$$

$$\frac{\psi^{(k)} - \psi^{(k-1)}}{\Delta t} \approx \frac{\partial \psi^{(k)}}{\partial t}, \tag{3.2}$$

where Δt is the size of the step taken and k is an index of time such that $t = k\ \Delta t$. For the second order spatial derivative of the single particle Hamiltonian one can make the approximation

$$\frac{\partial^2 \psi_j}{\partial x^2} \approx \frac{\psi_{j+1} - 2\psi_j + \psi_{j-1}}{\Delta x^2}\ , \tag{3.3}$$

where Δx is the spacing of the grid and j is the grids index such that $x = a + j\Delta x$, where a is the lowest value of the grid. Replacing the wavefunction itself with its their

finite difference expression, we obtain

$$\frac{i\hbar}{2m\Delta x^2}(\psi_{j+1}^{(k)}+\psi_{j-1}^{(k)}-2\psi_j^{(k)})-\frac{i}{\hbar}V(a+j\Delta x)\psi_j^{(k)}=\frac{\psi_j^{(k+1)}-\psi_j^{(k)}}{\Delta t}\ . \tag{3.4}$$

The Hamiltonian can be solved in two different ways depending on the purpose. To find the eigenstates requires one to consider the time independent case and the left hand side of the equation can be solved using exact diagonalization. To follow the dynamics of the state over time, the time dependent case is considered and the whole equation is discretized with particular emphasis on the right hand side using the Crank-Nicolson method [80]. To illustrate this, I will start by detailing the formalism of exact diagonalization to show how one can find the eigenstates of a Hamiltonian

3.1.1 Exact Diagonalization

While exact analytical solutions are only available for a very small number of select Hamiltonians in quantum mechanics, for benign systems the eigenstates and eigenspectrum can usually be obtained numerically using the exact diagonalization method. For this, a given Hilbert space needs to be truncated so that it is spanned by a suitable, finite basis of N states. The Hamiltonian can then be expanded in this basis and takes the form of a finite-sized matrix, which can be numerically diagonalized and the eigenstates and eigenfunctions one finds correspond to the eigenstates and eigenspectrum of the Hamiltonian.

Starting with the single particle Hamiltonian

$$H=-\frac{\hbar^2}{2m}\frac{\partial^2}{\partial x^2}+V(x)\ , \tag{3.5}$$

one can approximate the spatial derivative as given in Eq. (3.3). It is to note that in the position basis it is important to have enough spatial resolution, Δx, to resolve the oscillations of the higher lying states, as the precision of this procedure depends on the size of the basis taken into consideration: states that are closer to the cut-off energies will be less accurate. In the matrix representation, writing the potential terms of the Hamiltonian in the discrete spatial basis is straightforward as these are already diagonal. The kinetic energy terms then make this matrix tridiagonal, leading to

$$\hat{H}=-\frac{\hbar^2}{2m\Delta x^2}\begin{pmatrix}-2 & 1 & 0 & \dots & 0\\ 1 & -2 & 1 & \ddots & \vdots\\ 0 & \ddots & \ddots & \ddots & 0\\ \vdots & \ddots & 1 & -2 & 1\\ 0 & \dots & 0 & 1 & -2\end{pmatrix}+\mathrm{diag}(V(x_1),V(x_2),V(x_3)...V(x_N))\ . \tag{3.6}$$

This simple matrix can then be diagonalized using built-in functionality in, e.g, MATLAB in order to find the eigenfunctions and eigenvalues for a Hamiltonian for any potential $V(x)$. To increase the accuracy of the derivative, either the number of grid points considered in the spatial derivative can be increased, or a higher order finite

difference scheme can be used [81]

$$\frac{\partial^2\psi}{\partial x^2} \approx \frac{-\psi_{j+2} + 16\psi_{j+1} - 30\psi_j + 16\psi_{j-1} - \psi_{j+2}}{12\Delta x^2} \,. \tag{3.7}$$

The trade off of using a higher order scheme is that the spatial derivative is no longer tridiagonal and requires a longer time to solve for a given basis. However this can be mitigated again using sparse matrix functions in MATLAB to reduce the amount of memory used in the diagonalization process.

3.2 Time-evolution of quantum states

In the Schrödinger picture the evolution of a quantum state $|\Psi(t)\rangle$ can be described using a unitary time-evolution operator, $U(t, t_0)$, such that

$$|\Psi(t)\rangle = U(t, t_0)|\Psi(t_0)\rangle, \tag{3.8}$$

where $t > t_0$. The wavefunction itself can be expanded into an orthonormal basis set $|\psi_n\rangle$

$$|\Psi\rangle = \sum_n c_n|\psi_n\rangle \,, \tag{3.9}$$

with $c_n = \langle\psi_n|\Psi\rangle$. The time evolution operator follows from the formal integration of Schrödingers equation as

$$U(t, t_0) = \exp\left(\frac{-i\mathcal{H}(t - t_0)}{\hbar}\right), \tag{3.10}$$

$$= \exp\left(\frac{-i\mathcal{H}\Delta t}{\hbar}\right) \,, \tag{3.11}$$

where $\mathcal{H}$ is the Hamiltonian operator of the system and Δt is the change in time $\Delta t = t - t_0$. A Taylor series expansion can be applied to the unitary operator to write it in the form

$$U(t, t_0) = 1 - \frac{i\mathcal{H}\Delta t}{\hbar} + \mathcal{O}(\Delta t^2) \,. \tag{3.12}$$

where $\mathcal{O}(\Delta t^2)$ is the error acquired from the expansion. Typically the error can be a problem when evolving the system, as the scheme does not preserve time reversal symmetry [82]. This problem is exasperated when the length of time simulated and the number of time steps required to break up a unitary operator becomes very large, where

$$U(t, 0) = \prod_{i=0}^{N-1} U(t_i + \Delta t_i, t_i) \,. \tag{3.13}$$

As a result keeping the system unitary over many time-steps becomes an issue. However one can choose a numerical scheme motivated by finite difference methods in order to mitigate the error of the evolution [83]. This insures the norm the wavefunction remains conserved.

3.2.1 Crank-Nicolson Method

The forward and backwards methods are simple methods to calculate the evolution of a wavefunction, however this comes at a few disadvantages. In the forward difference method in Eq. (3.1) the method is classified as explicit, meaning the state at time $t+\Delta t$ is solved with the information of the state at time t. This is very intuitive however incurs a large error if the time step taken is not small enough. Over long run times of the simulations the stability therefore needs to be carefully checked. The backwards difference method in Eq. (3.2) is an implicit method to find a solution for the state at the current time t and at a time of $t+\Delta t$. This method is considered unconditionally stable, however is computationally expensive. A good compromise between the drawbacks of these two schemes is to use an averaging of both time evolution schemes as in the Crank-Nicolson approach [83, 84].

For this one starts with the forward method in Eq. (3.1) and rewrites the Hamiltonian as

$$\begin{aligned} \frac{\psi_j^{(k+1)} - \psi_j^{(k)}}{\Delta t} &= \frac{i}{\hbar} H_j \psi_j^{(k)}, \\ \psi_j^{(k+1)} &= \psi_j^{(k)} (1 + \frac{i}{\hbar} H_j \Delta t) \ . \end{aligned} \tag{3.14}$$

Similarly the backwards method in Eq. (3.2) can be written as

$$\psi_j^{(k)} = (1 - \frac{i}{\hbar} H_j \Delta t) \psi_j^{(k+1)} \ , \tag{3.15}$$

where for the purpose of keeping similar indices $k \to k+1$. Both of these methods can then be averaged such that

$$\left(1 - \frac{i}{\hbar} \frac{H\Delta t}{2}\right) \psi_j^{(k+1)} = \psi_j^{(k)} \left(1 + \frac{i}{\hbar} \frac{H\Delta t}{2}\right) \ . \tag{3.16}$$

The single order approximation now turns into a second order algorithm with a discretization error that decreases with $\mathcal{O}(\Delta t^2)$.

Part II

Nonequilibrium Dynamics and Quantum Control

Chapter 4

Nonequilibrium many-body dynamics in supersymmetric systems

4.1 Introduction

In this Chapter I will expand on the mathematical tools used in my publication titled "Nonequilibrium many-body dynamics in supersymmetric quenching" [1] and highlight some of the results. A quench is a process in which a many-body system is subjected to a sudden change in its Hamiltonian, $\mathcal{H} \to \mathcal{H}'$, which drives the system from its initial stationary state into a nonequilibrium one, $\Psi(t) = e^{-i\mathcal{H}'t}\Psi(t=0)$. Quench protocols are commonly used to study the response of quantum systems to perturbations as they allow to probe the excitation spectrum, which can be then be used to study nonequilibrium thermodynamic quantities such as the work statistics [85, 86] many-body effects such as thermalization [87] or the orthogonality catastrophe [88]. They also provide an experimental framework to study many-body localization [89–91]. Ultracold atoms are perfectly suited to study nonequilibrium phenomena as modern experiments allows for the accurate measurement of athe density of a gas through time-of-flight measurements [92], while different interferometric techniques can be used to quantify the amount of nonequilibrium excitations [93–95].

The degree of control in modern cold atom experiments allows for the modification of nearly all parts of the systems Hamiltonian, offering different avenues to implement sudden quenches. The two most common quenches correspond to either a sudden change in the interactions between particles or the strength of the external trapping potential. A quench of the interactions between particles can significantly change the energy spectrum in a non-trivial manner which can lead to complex dynamics and the destruction of revivals of the initial state [19, 96]. On the other hand a quench of the potential itself, such as the frequency of a harmonic oscillator [97] or expanding power law traps [98], can produce scale invariant dynamics even for many-body Bose [99] and Fermi gases [100, 101]. In fact the density and momentum distribution can be tracked from these types of quenches, where once the trap frequency is changed the emergence of excitations in the form of breathing modes can occur in many-body systems [102–104]. In this Chapter I will explore the dynamics and calculations associated with a quench of the latter kind, specifically using a quench between the infinite square well

(ISW) and its supersymmetric partner potentials.

While quenching of a trapping potential often means changing only one parameter, such as the trap frequency of the harmonic oscillator or the length of an ISW, this preserves the functional form of the potential. For quenches involving purely the expansion of an ISW one would expect perfect periodic revivals for both non-interacting fermions and the Tonks-Girardeau gas [105], which is the analog of the well-known Talbot effect in optics [106, 107]. However, the dynamics following an arbitrary quench can be a lot more complex, especially in many-body systems, and it is important to identify situations where different effects can be clearly attributed to different phenomena. Quenching between supersymmetric potentials allows one to make an important simplification, as the eigenspectra before and after the quench are (mostly) identical. However, the shape of the potential is different and so are their eigenstates, meaning the wave-function overlaps can play a more important role in the dynamics. Furthermore, the fact that the factorisation operators can be used to transform the eigenstates between the different supersymmetric Hamiltonians (see Eqs. (2.15) and (2.16)) can allow one to obtain analytical expression for some of the observables after the quench [74].

Specifically, the work presented in this Chapter explores the nonequilibrium dynamics of a one-dimensional Fermi gas that is initially prepared in an infinite square well which is subsequently quenched to a higher order supersymmetric partner potential. To start I will introduce the non-interacting Fermi-gas, and after that I will expand on the two quantities used throughout the work: the survival probability and the work probability distribution. Through these I will explore how supersymmetry influences the resulting dynamics.

4.2 Degenerate Fermi Gas

For this work I consider a degenerate spin polarized Fermi gas of N particles in a one-dimensional ISW trap, $V(x_1, x_2, ..., x_N)$. The many-body Hamiltonian can be written as

$$\mathcal{H} = \sum_{i=1}^{N} \left[-\frac{\hbar^2}{2m} \nabla_i^2 + V(x_i) \right], \tag{4.1}$$

and the many-body wavefunction and energy are determined by $\mathcal{H}\Psi = \mathcal{E}\Psi$. Since I consider a non-interacting gas, the many-body wavefunction can be written as a product of single particle wavefunctions $\psi_i(x_j)$

$$\Psi(x_1, x_2, ..., x_N) = \psi_1(x_1)\psi_2(x_2)...\psi_N(x_N) \ , \tag{4.2}$$

however for a gas of identical particles the coordinates exchange operator P needs to be included to account for all permutations

$$P_{ij}\Psi(x_1, \ldots, x_i, \ldots, x_j, \ldots, x_N) = \pm\Psi(x_1, \ldots, x_j, \ldots, x_i, \ldots, x_N), \tag{4.3}$$

where the $\pm$ denotes the symmetric or anti-symmetric nature of the wavefunction. For an N particle Fermi gas this can be accounted for by writing the many-body

wavefunction as a Slater determinant of single particle states as

$$\Psi\left(x_1, x_2, ..., x_N\right) = \frac{1}{\sqrt{N!}} \det_{i,j=1}^{N} \left[\psi_i(x_j)\right] , \tag{4.4}$$

where the states ψ_i can be found by solving the single-particle TISE

$$H\psi_i = \left[-\frac{\hbar^2}{2m}\nabla^2 + V(x)\right]\psi_i = E_i\psi_i \ . \tag{4.5}$$

For a spin-polarized Fermi gas the Pauli exclusion principle enforces that only one fermion can occupy each energy level, such that the ground state at zero temperature has the lowest N levels occupied with total energy $\mathcal{E}_0 = \sum_{i=1}^{N} E_i$. At very low temperatures the many-body state has therefore a hard boundary in energy space, known as the Fermi edge, which is the transition point between occupied and unoccupied states [108, 109].

In the presence of finite temperature the Fermi edge melts away and is replaced with a smooth continuous distribution of particles over all states. For single particle states of energy E_i the average occupation number $\hat{n}_i$ is

$$\hat{n}_i = \frac{1}{e^{(E_i-\mu)\beta} + 1}, \tag{4.6}$$

where β is the inverse of the temperature multiplied by the Boltzmann constant, $\beta = (k_b T)^{-1}$, and μ is the chemical potential of the system and $\sum_{i=1}^{\infty} \hat{n}_i = N$.

4.3 An Overview on Quench Dynamics

In this Section I will give a brief overview of the main quantities used in my work, i.e. the survival probability and the work probability distribution (WPD). I will show how the survival probability for non-interacting fermions can be significantly simplified by taking advantage of the description of the many-body fermionic wavefunction in terms of single particle states. I will then outline how intertwining relationships and wavefunction transformations developed in Chapter 2 can be used to simplify a quench between partner potentials. Lastly I will use the WPD to decompose and identify the nonequilibrium excitations in the system for both a generic and a SUSY quench.

4.3.1 Survival Probability

When a system is quenched the initial wavefunction undergoes out-of-equilibrium dynamics governed by its new Hamiltonian. During the evolution the wavefunction often exhibits dynamics which increases in complexity and leads to decoherence of the system [110, 111]. An important quantity to explore different aspects of an evolving state is the survival probability, which is also known as the Loschmidt Echo [112, 113]. For a continuously evolving state, the survival probability is a gauge of the orthogonality between the time evolved state and the initial state pre-quench, written as $F(t) = |\langle\Psi(0)|\Psi(t)\rangle|^2$. In the case where the survival probability is zero, the two wave-

functions are orthogonal to each other [88] and therefore this quantity can be used to measure how far a state is driven away from equilibrium.

Zero temperature

At zero temperature the ground state of a spin-polarised Fermi gas consisting of N particles is given by a Fermi sea in which all eigenstates of the single-particle Hamiltonian $H^{(1)}$ are filled from the lowest lying states up to N-th state with exactly one particle. For a pure state the survival probability in terms the many-body wavefunction is written as

$$F(t) = |\mathcal{O}(t)|^2 = \left| \langle \Psi_0^{(1)} | e^{-i\mathcal{H}^{(1)}t} e^{i\mathcal{H}^{(2)}t} | \Psi_0^{(1)} \rangle \right|^2 , \tag{4.7}$$

where $\Psi_0^{(1)}$ is an eigenstate of the Hamiltonian $\mathcal{H}^{(1)}$ and $\mathcal{H}^{(2)}$ is the quenched Hamiltonian. The overlap allows one to study intrinsic effects such as the orthogonality catastrophe, an effect that arises when a system is subjected to a sudden perturbation [88]. It predicts that the evolved many-body state of the gas becomes more and more orthogonal to the initial state with increasing particle number [18, 114, 115]. However, since $\Psi_0^{(1)}$ is the N-body wavefunction of a gas of non-interacting fermions, calculating the overlap between two many-body states in Eq. (4.7) quickly becomes numerically intractable for large N. However, one can take advantage of the properties of the Slater determinant (see Eq. (4.4)) which allows to rewrite the many-body overlap in terms of more accessible single particle overlaps

$$\mathcal{O}(t) = \det[\mathbf{O}(t)] , \tag{4.8}$$

with the overlap matrix for N-particles given by

$$\mathbf{O}(t) = \begin{pmatrix} \mathcal{O}_{11} & \mathcal{O}_{12} & \dots & \mathcal{O}_{1N} \\ \mathcal{O}_{21} & \mathcal{O}_{22} & \ddots & \vdots \\ \vdots & \ddots & \ddots & \vdots \\ \mathcal{O}_{N1} & \dots & \dots & \mathcal{O}_{NN} \end{pmatrix} , \tag{4.9}$$

and the elements being the single particle overlaps

$$\mathcal{O}_{kl} = \langle \psi_l^{(1)} | e^{-iH^{(1)}t} e^{iH^{(2)}t} | \psi_k^{(1)} \rangle . \tag{4.10}$$

Here, $\psi_l^{(1)}$ are single particle eigenstates of $H^{(1)}$, and $H^{(2)}$ is the quenched single particle Hamiltonian. Inserting a completeness relation for the eigenstates of $H^{(2)}$ gives

$$\mathcal{O}_{kl} = \sum_{m=1}^{\infty} \langle \psi_l^{(1)} | e^{-iH^{(1)}t} | \psi_m^{(2)} \rangle \langle \psi_m^{(2)} | \psi_k^{(1)} \rangle e^{iE_m^{(2)}t}, \tag{4.11}$$

so that the overlap matrix elements can be written as [18, 114, 116]

$$\mathcal{O}_{kl} = \sum_{m=1}^{\infty} \langle \psi_l^{(1)} | \psi_m^{(2)} \rangle \langle \psi_m^{(2)} | \psi_k^{(1)} \rangle e^{-i(E_l^{(1)} - E_m^{(2)})t}, \tag{4.12}$$

where $E_l^{(1)}$ and $E_m^{(2)}$ are the single particle energies of $H^{(1)}$ and $H^{(2)}$. This description of the many-body overlap now allows to compute the survival probability for larger numbers of particles without too much computational resources required.

Finite temperature

To describe the dynamics of a system at finite temperatures, the initial state has to be described by a density matrix given by a Gibbs distribution

$$\rho_0 = \frac{e^{-\mathcal{H}^{(1)}\beta}}{Z}|\Psi\rangle\langle\Psi| \,, \tag{4.13}$$

where $Z = \sum_n e^{-\beta E_n}$ is the grand canonical partition function. The survival probability, $F(t)$, after a quench then becomes

$$F(t) = |\mathcal{O}(t)|^2 = \left|\mathrm{Tr}\left[\rho_0 e^{-i\mathcal{H}^{(1)}t} e^{i\mathcal{H}^{(2)}t}\right]\right|^2 \,. \tag{4.14}$$

Similar to the many-body wavefunction at $T = 0$, Levitov and Lesovik [117] showed that the trace of the many-body Hamiltonian can also be written as a determinant of the single particle Hamiltonian using the trace formula $\mathrm{Tr}\left[e^{-i\mathcal{H}^{(1)}t} e^{i\mathcal{H}^{(2)}t}\right] = \det\left[1 + e^{-iH^{(1)}t} e^{iH^{(2)}t}\right]$. The overlap in Eq. (4.14) then becomes

$$\mathcal{O} = \det\left[1 - \hat{n}_i + \hat{n}_i e^{-iH^{(1)}t} e^{iH^{(2)}t}\right], \tag{4.15}$$

where $\hat{n}_i$ is the Fermi-Dirac distribution from Eq. (4.6). Writing the trace in this form again only requires the calculation of single particle overlap matrix elements, and of course taking $T = 0$ reduces the calculation to the elements of Eq. (4.12).

The expression above was developed to account for the full counting statistics found in charge transport and the distribution of shot noise. However, it has also recently found use in describing the overlap dynamics of non-interacting Fermi gases as a measure of decoherence [118–120]. Experimentally the overlaps can be probed using radio frequency spectroscopy techniques and Ramsey interferometry, and have been used to track the nonequilibrium dynamics of quenched Fermi gases [93, 94, 121]. Here a $\pi/2$ pulse is applied to the impurity atoms which puts them into a superposition of two internal Zeeman states, which interact differently with the Fermi gas. This induces nonequilibrium dynamics in the Fermi gas which can be probed by applying a further $\pi/2$ pulse at a later time and measuring the probability for the impurities to be either in their ground or excited states. This then allows to extract the many-body overlap of Eq. (4.7). These techniques have also been shown to allow to use the overlap for the precise measurement of temperature in ultracold Fermi gases [122, 123].

4.3.2 Quenching with SUSY potentials

The Hamiltonians I use in the quenches discussed below are constructed using the supersymmetric factorization methods. This means that the eigenspectrum is mostly

unchanged during a quench, apart from the removal (or addition) of the ground state level. Furthermore adjacent and iterated intertwining properties exist between supersymmetric potentials, which will allow to write the overlap matrix elements purely in terms of the original potential. This can be done by taking the wavefunctions of the target potential $\psi_n^{(2)}$ and using the supersymmetric operator $A^{(1)}$ in order to write the wavefunction in terms of $\psi^{(1)}$ by using the transformation Eq. (2.16). Once this is accomplished, the intertwining property of the time evolution, see Eq (2.20), allows us to also write the energy in the exponential term $e^{-\frac{i}{\hbar}E_m^{(2)}t}$ in terms of the original spectrum.

With these considerations, starting with the elements of the overlap matrix in Eq (4.12), the overlap elements for SUSY partner potentials can be written as

$$\mathcal{O}_{kl} = \sum_{m=1}^{\infty} \langle \psi_l^{(1)} | A^{(1)} | \psi_{m+1}^{(1)} \rangle \langle \psi_{m+1}^{(1)} | A^{(1)\dagger} | \psi_k^{(1)} \rangle \frac{e^{-\frac{i}{\hbar}\left(E_{m+1}^{(1)} - E_l^{(1)}\right)t}}{\Delta E_{m+1}} \,. \tag{4.16}$$

where $\Delta E_{m+1} = E_{m+1}^{(1)} - E_1^{(1)}$. The survival probability can then be calculated using Eq. (4.8).

For higher order potentials on the other hand, for example a quench between the initial potential $V^{(1)}$ and its second partner potential $V^{(3)}$, we implement the same steps as before for a wavefunction transformation and then apply the unitary intertwining property sequentially. If we start with a wavefunction basis of the second second partner potential $\psi_m^{(3)}$ the overlap matrix elements can be written as

$$\mathcal{O}_{kl} = \sum_{m=1}^{\infty} \langle \psi_l^{(1)} | A^{(2)} A^{(1)} | \psi_{m+2}^{(1)} \rangle \langle \psi_{m+2}^{(1)} | A^{(1)\dagger} A^{(2)\dagger} | \psi_k^{(1)} \rangle \frac{e^{-\frac{i}{\hbar}\left(E_l^{(1)} - E_{m+2}^{(1)}\right)t}}{\Delta E_{m+2}^{(1)} \Delta E_{m+1}^{(2)}} \,. \tag{4.17}$$

The derivations provided are kept general as they applies to all SUSY potential hierarchys and are not exclusive to the infinite square well.

4.3.3 Work Probability Distribution

The dynamical overlap $\mathcal{O}(t)$ not only describes the distinguishability of the nonequilibrium and initial states, but is also related to the work statistics of the quench dynamics [101, 124–126]. In particular, the initial decay of $\mathcal{O}(t)$ can quantify the moments of the work distribution [127], with the average work done by the quench given by

$$\langle W \rangle = -i \partial_t \mathcal{O}(t)|_{t=0} \,. \tag{4.18}$$

Here $\mathcal{O}(t)$ is known as the characteristic function of the work probability distribution (WPD) which is given by

$$\mathcal{O}(t) = \int dt \, e^{iWt} P(W), \tag{4.19}$$

where $\mathcal{O}(t) = \sum_n |\langle\Psi_n^{(\alpha)}|\Psi_0^{(1)}\rangle|^2 e^{-i(\mathcal{E}_n^\alpha - \mathcal{E}_0^{(1)})t}$ can be written as the full sum of the many-body overlaps. Here we have started by taking the $T = 0$ case and considering the initial many-body groundstate $\Psi_0^{(1)}$. Rearranging Eq. (4.19) and differentiating with respect to t such that $-i\partial_t\mathcal{O}(t)|_{t=0}$, allows to obtain the work probability distribution as

$$P(W) = \sum_n |\langle\Psi_n^{(\alpha)}|\Psi_0^{(1)}\rangle|^2 \, \delta\,(W - (\mathcal{E}_n^\alpha - \mathcal{E}_0^{(1)})). \tag{4.20}$$

The WPD is measured using two point measurement in time of the probability to find a system in a particular state after the quench [101, 124–126]. This allows one to understand the spread of the excitations as a system is quenched to the final Hamiltonian. It is comprised of the probability of finding the ground state of a Fermi gas at $t = 0$ with energy $\mathcal{E}_0^{(1)}$ in a state $\Psi_n^{(\alpha)}$ of the potential α after the quench. The delta term then ensures the conservation of energy as the amount of work required, W, to bring an ensemble of fermions from the ground state to an excited ensemble n must equal the difference in energy of the two states, i.e. $W = \mathcal{E}_n^{(\alpha)} - \mathcal{E}_0^{(1)}$. The energy of each state is simply the sum of the single particle energies which the gas occupies. For the ground state this is simply $\mathcal{E}_0^{(1)} = \sum_{n=1}^N E_n^{(1)}$ where as for the excited ensemble this is $\mathcal{E}_n^{(\alpha)} = \sum E_{n_i}^{(\alpha)}$ where $\{n_i\}_{1,2,\ldots,N}$ are a set of quantum numbers for the single particle states that make up $\Psi_n^{(\alpha)}$.

For an N-particle Fermi gas at $T = 0$ excitations are limited to the very edge of the Fermi sea. At finite temperature the Fermi edge melts away opening the Fermi sea and the thermal distribution of the states before quenching needs to be accounted for [101, 122, 128]. The initial thermal distribution of states is calculated using the Gibbs factors $p_s^{(1)} = \frac{1}{Z_0} e^{\beta(\mathcal{E}_s^{(1)} - N\mu)}$, where Z_0 is the grand-canonical partition function and $\{s_j\}_{1,2,\ldots,N}$ are single particle quantum numbers for the initial state. The WPD then simply changes to account for this distribution

$$P(W) = \sum_s \sum_n p_s^{(1)} \left|\langle\Psi_n^{(\alpha)}|\Psi_s^{(1)}\rangle\right|^2 \delta\left(W - \left(\mathcal{E}_n^{(\alpha)} - \mathcal{E}_s^{(1)}\right)\right). \tag{4.21}$$

Due to the conservation of energy SUSY potentials offer an advantage to the calculation of the WPD due to the degeneracy of potentials in the SUSY hierarchy. After the Fermi gas is quenched, particles in the quenched system will occupy states of the same energy as the initial system. The difference in energy is then the difference of occupied single particle states that are not degenerate with one another. For example, the energy difference of the groundstate transition $\left|\langle\Psi_0^{(2)}|\Psi_0^{(1)}\rangle\right|^2$ after a quench between $V^{(1)} \to V^{(2)}$ is simply the energy difference between the non-degenerate occupied states, namely $\Delta\mathcal{E} = E_N^{(2)} - E_1^{(1)}$. Similarly for a quench to $V^{(3)}$ this is the difference of the first two single particle states in $V^{(1)}$ and the last two single particle states of $V^{(3)}$, $\Delta\mathcal{E} = \sum_{n=N-1}^N E_n^{(3)} - \sum_{n=1}^2 E_n^{(1)}$.

4.4 Supersymmetric Quenching of the ISW

In my work [1] I consider a quench from an ISW to one of its partner potentials. As laid out in Section 4.3.2 when a system is prepared in any potential and quenched to one of its partner potentials, the resulting overlap matrix and its elements can be written in terms of the single particle states of the initial Hamiltonian. This is accomplished using a series of SUSY transformations on each of the wavefunctions between the initial and target potential. Figure 4.1 shows the change of different diagonal overlap elements $\mathcal{O}_{ii}(t)$ after a quench from the ISW to the first partner potential at $T = 0$. As one can see at different times post quench the overlaps have moments where the survival probability reaches $F(t) = 1$. For odd numbered overlaps however there are 4 times where this occurs (panels (a)), whereas for even numbered overlaps this occurs at 8 times (panel (b)). This is an effect which arises if the evolving wavefunction is of even or odd symmetry [129], leading to the observation of different numbers of revivals for different overlap elements. In the following sections we will expand on this by calculating the phase of the single particle overlaps at these revival times. The resulting survival probability for 10 particles calculated from Eq. (4.8) is plotted in panel (c). Since all individual overlap elements produce revivals at $t_r/4$ regardless of being odd or even, the resulting survival probability also produces revivals at $t = t_r/4$. This is further echoed in the probability density in panel (d), which is calculated as

$$\rho(x,t) = \sum_{n=1}^{N} |\psi_n^{(1)}(x,t)|^2 = \sum_{n=1}^{N} \left| \sum_m |\psi_m^{(2)}(x)\rangle\langle\psi_m^{(2)}(x)|\psi_n^{(1)}(x)\rangle e^{-\frac{i}{\hbar}(E_m^{(2)}-E_n^{(1)})t} \right|^2 , \quad (4.22)$$

and can be found in Figure 4.1 panel (d). This is an example of a quantum carpet [105, 130], a visual representation highlighting the Talbot effect in matter-waves [131–133].

The Talbot effect is a diffraction effect that occurs when an incoming plane wave is incident on a periodic diffraction grating. As a result a fractal pattern emerges at various distances from the diffraction grating. For matter waves on the other hand [134] the same diffraction pattern can be created as the wavefunction evolves over time [107, 135], providing an excellent way for studying the decoherence of a system [136]. In Figure 4.1 panel (d), at times of $t_r/4$ the probability density returns to its initial probability density, see panels (e) and (f) for example, producing similar fractal patterns to that of Talbot oscillations.

The revivals calculated for the SUSY ISW in Figure 4.1 are similar to different studies on atomic center-of-mass dynamics [105, 135, 136]. However, where our results differ is when the finite temperature regime is considered. At finite temperature for a generic symmetric expansion of an infinite box (e.g. the Talbot effect), the overlap elements dephase with one another. However, I have shown that the overlap elements for a SUSY quench remain in phase, which allows to see many-body revivals at long times. This highlights the benefit of using SUSY potentials, specifically for the case of the ISW. One of the clear differences between the two quenches is that the energy spectrum for the infinite box changes as the box expands from L_1 to L_2, while for the SUSY quenches the energy spectrum is unchanged. To obtain a full picture we have to explore the effect of SUSY on the time dependent term and build an understanding of

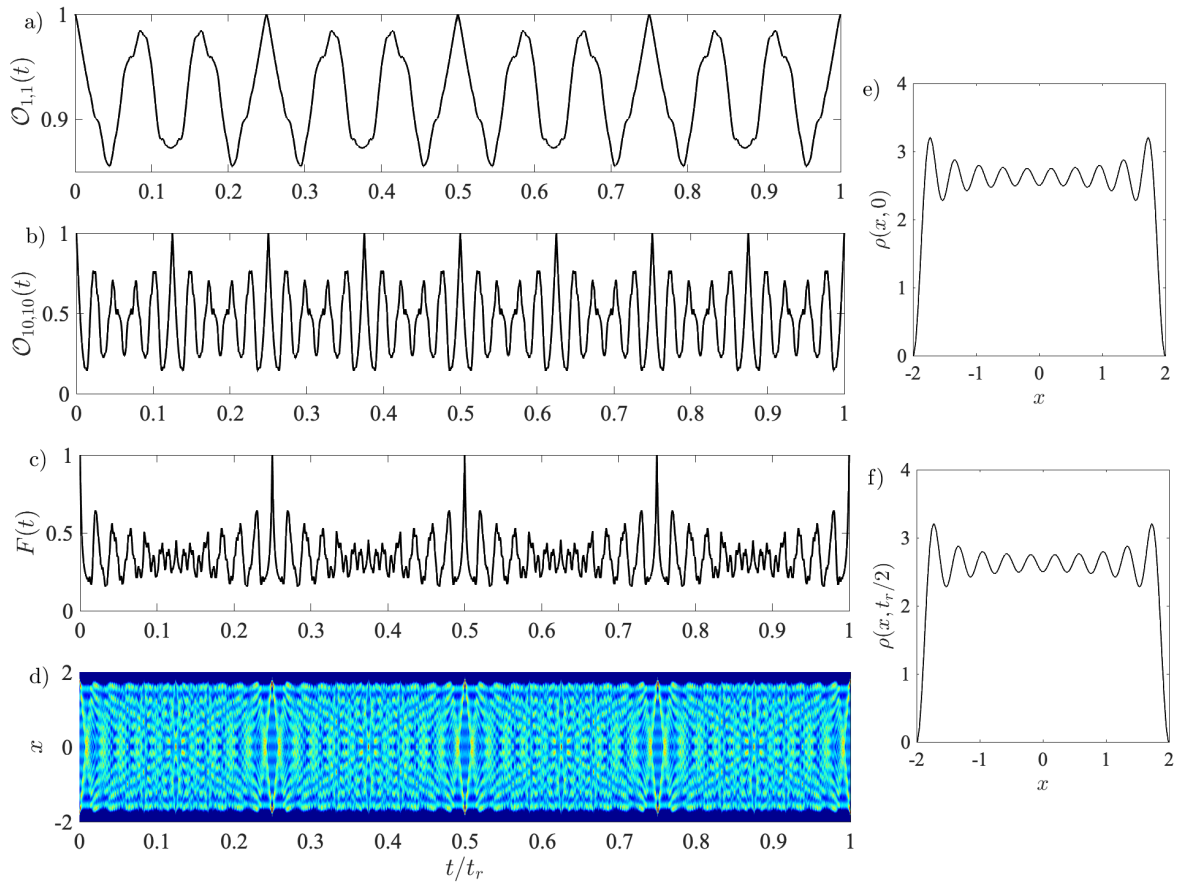

Figure 4.1: Dynamical overlaps of a) $\mathcal{O}_{1,1}$ b) $\mathcal{O}_{10,10}$ with c) the resulting survival probability and d) probability density $\rho(x,t)|$. From the survival probability the density of the system is plotted for time e) $t = 0$ and f) $t = t_r/2$. For all plots a 10 particle Fermi gas is quenched from the ISW to the first partner potential at $T = 0$.

1) where these revivals come from and 2) why do SUSY quenches retain them at finite temperature.

4.4.1 Quantum Revivals

Quantum revivals have been present in a number of systems, for example in the collapse and recombination of Rydberg wavepackets which were found to reform close to their original shape [137, 138]. Such revivals are, however, not limited to the specific example settings, but can be described generically as done by Bluhm *et al.* in 1996 [139]. In fact, the study of wavefunction revivals is a fundamental problem in quantum mechanics [135, 140–143] and are most prominently manifested in the aforementioned Talbot effect, where in the time-evolution of the probability density [105] revivals and fractional revivals [140] appear.

To look at this more closely, one can consider the revival time for a single particle state in an infinite box. Bluhm *et al.* showed [139] that by considering a particle excited to some mean but predominant excitation level around $\tilde{n}$, weighted probabilities can

be used to model the approximate energy of this wavepacket. In particular, the energy can be written using a Taylor expansion with respect to the principle quantum number of the form

$$E_n \approx E_{\tilde{n}} + E'_{\tilde{n}}\,(n-\tilde{n}) + \frac{1}{2}E''_{\tilde{n}}\,(n-\tilde{n})^2 + \frac{1}{6}E'''_{\tilde{n}}\,(n-\tilde{n})^3 + \dots\ . \tag{4.23}$$

From this expansion one can obtain different time scales which define various periods of the system, such as the classical period (T_{cl}), the revival time (t_r)and the super-revival time (t_{sup}),

$$T_{cl} = \frac{2\pi}{|E'_{\tilde{n}}|} \quad t_r = \frac{4\pi}{|E''_{\tilde{n}}|} \quad t_{sup} = \frac{12\pi}{|E'''_{\tilde{n}}|}\ . \tag{4.24}$$

When the survival probability is measured over time these time scales can be observed as recurrences of the initial state can be identified after being released into a potential where it is allowed to evolve. For example, in [144] the connection between the survival probability and the classical period is made using autocorrelation functions, calculated using the inner product of the time-evolved wavefunction with its state before evolution.

Returning to the ISW, the energy spectrum for a system of width L centered around the origin is given by

$$E_n = \frac{n^2\pi^2\hbar^2}{2mL^2}. \tag{4.25}$$

Taking the second derivative of the energy,

$$\frac{\partial^2 E}{\partial n^2} = \frac{4\pi^2\hbar^2}{mL^2}, \tag{4.26}$$

allows to obtain the revival time as

$$t_r = \frac{4L^2}{\pi}, \tag{4.27}$$

where we have set $\hbar = m = 1$. This is an important result because it indicates that a wavefunction, irregardless of the state it occupies, will return to its original initial state. For a Fermi-gas of N particles trapped in an ISW potential where each state is occupied by one particle, all states will return to their initial state at the same time. Even though for an expanding box two different times can be calculated for each set of wavefunctions, which are proportional to the box lengths L_1 to L_2, it is clear that revivals still occur in accordance with the target potentials box length. In the context of supersymmetry, since the SUSY partner potentials of the ISW possesses the same eigenspectra and have the same dependency on L, revivals in the system will appear as if the gas was simply evolving in just the box. This, however, changes when temperature is included and the thermal occupation numbers of the states are taken into account.

Other time scales manifest in the survival probability in different ways. For a particle in a harmonic oscillator the classical period can be observed at intervals of $\frac{\pi}{\omega}$ after a trap frequency quench [18, 97]. There is no dependence on the state for the classical period in the same way that there is no dependence on the revival time for the ISW. The classical period for the ISW does, however, have a dependence on the

state a particle is evolving in. This means that for an N body system the survival probability exhibits smaller, weak revivals in between the predominant revivals, as the contribution of constructive/destructive interference arises from differing classical periods. It is therefore important to look at the phase and we will explore this in the next section.

4.4.2 Revival Retention in Survival Probability

So far we have calculated the revival times for single particle states [144]. For the ISW this time scale is not state dependent and is only dependent on the length of the potential. By quenching to a potential within a SUSY hierarchy of the ISW this time scale is preserved and the single particle states evolve as if they are evolving in the original potential. However to consider the phase the difference in energy of the single particle states between potentials needs to be to be taken into account [110, 111], see Eq. (4.12).

To start let us emphasise that an even-odd effect occurs in the evolution of the quantum states for the ISW [129]. Therefore, it is useful for us to separate the eigenspectra of the ISW into the ones with even and with odd energies as

$$E_n^e = E_1(2n+1)^2 \quad \text{and} \quad E_n^o = 4E_1(n+1)^2\,, \tag{4.28}$$

for $n = 0, 1, 2, 3\ldots$. This translates into the expression for the phase dependence of the exponential term of the overlap as

$$e^{-\frac{i}{\hbar}E_n^e t} = e^{-i\phi_n^e(t)} = e^{-\frac{2\pi i(2n+1)^2}{t_r}t}\,, \tag{4.29}$$

$$e^{-\frac{i}{\hbar}E_n^o t} = e^{-i\phi_n^o(t)} = e^{-\frac{8\pi i(n+1)^2}{t_r}t}\,. \tag{4.30}$$

For $t = t_r$ it is easy to see that the revival time simply becomes an integer multiple of 2π which produces a revival in the survival probability. For our quenches however, one can see that revivals occur at times of $t = t_r/4$ for even states and $t = t_r/8$ for odd states [129], which relates to the phases being independent of n

$$\phi_n^e(t_r/4) = \frac{\pi}{2} \pmod{2\pi}, \tag{4.31}$$

$$\phi_n^o(t_r/4) = 0 \pmod{2\pi}\,. \tag{4.32}$$

This result is straightforward to derive however we are interested in the difference of the phases, in particular the difference in phase of the diagonal of the overlap matrix $\mathcal{O}_{ii}(t)$. The diagonal of the overlap matrix will have much larger contributions compared to the off-diagonal elements. For the overlap of even and odd states these elements go to zero and for same parity states of different order the overlap is usually small. For a quench between partner potentials, for example $V^{(1)} \to V^{(2)}$ (or every quench where the difference in the order of the supersymmetric partner potentials is odd), the diagonal elements $\mathcal{O}_{ii}(t)$ describe a transition from a state with an even quantum number to one with an odd quantum number in the hierarchy's original basis, and the phases of

the overlap matrix elements in Eq. (4.16) can be written as

$$\Delta\phi = \phi^{\mathrm{e,o}}\left(\frac{t_r}{4}\right) - \phi^{\mathrm{o,e}}\left(\frac{t_r}{4}\right) = \pm\frac{\pi}{2} \pmod{2\pi} . \tag{4.33}$$

For a quench between the original potential and the next-next potential, i.e. $V^{(1)} \to V^{(3)}$, the overlap matrix for the diagonal in this case is

$$\Delta\phi = \phi^{\mathrm{e,o}}\left(\frac{t_r}{4}\right) - \phi^{\mathrm{e,o}}\left(\frac{t_r}{4}\right) = 0 \pmod{2\pi} . \tag{4.34}$$

The above example is specific to the ISW, however systems with eigenspectra that have an n^2 dependence can be treated in a similar way. This dependence leads to a common revival time t_r for all eigenstates and for all potentials in the hierarchy. For revival times that are state dependent, on the other hand, this calculation of the phase is not as straightforward. The effects of having state dependent time scales in regards to the survival probability will be discussed in section 4.6.1, where the survival probability for a quench between partner potentials containing the superpotential $\mathcal{W}(x) = x^3$ is described.

4.5 Publication

The results of Chapter 4 using the ISW as an example are published as:

Christopher Campbell, Thomás Fogarty and Thomas Busch
Nonequilibrium many-body dynamics in supersymmetric quenching
Phys. Rev. Research 4, 033014 (2022) [1]

I derived all the analytical results for the supersymmetric intertwining relationships for the survival probability and description of the phase factor, as well as performed all numerical simulations and identification of transitions for the work probability distribution. I also produced the first draft of the paper and all authors contributed to discussion, interpretation of results and final production of the material published.

4.6 Remarks

The primary potential I have used for my publications and this thesis is the ISW. Analytical expressions for this potential are known and a detailed description of the SUSY hierarchy of the potentials is well documented [60]. This allows us to exploit the intertwining properties and simplify different expressions and quantities such as the transformation of wavefunctions, creation of partner potentials and deriving values such as the revival time. The ISW is also a potential that has been well studied in the realm of nonequilibrium dynamics and wavefunction revival and fractional revival dynamics alike. It is, however, interesting to compare the results obtained for the ISW to other supersymmetric potentials. While we do not have the convenience of having an analytical expression for the ground state available for every potential we

can start by choosing a superpotential that will ensure the two potentials produce the same eigenspectra. I will do this for two different superpotentials, $\mathcal{W}(x) = x^3$ and $\mathcal{W}(x) = A\tanh(x/a)$.

4.6.1 $\mathcal{W}(x) = x^3$

To start I choose a system for which no analytical solutions exist. I specify a superpotential and create two potentials which, as usual, have identical eigenspectra, with one potential containing an extra state below the ground state of the higher order one. My system of choice is

$$\mathcal{W}(x) = x^3 \,, \tag{4.35}$$

as this leads to potentials that have normalizable ground state wavefunctions given by

$$V^{(1)} = x^6 - \frac{3}{\sqrt{2}}x^2 \quad \text{and} \quad V^{(2)} = x^6 + \frac{3}{\sqrt{2}}x^2 \,. \tag{4.36}$$

For these potentials the eigenspectra are not known analytically, but for a general power-law trap (i.e. $V(x) = x^k$), the state dependence of the energy spectra is known to be [145–147]

$$E_n \propto n^{2k/(k+2)}. \tag{4.37}$$

For the harmonic oscillator where $k = 2$, this leads to the expected linear spectrum, while for $k = 6$ the dependence is $n^{3/2}$. Using this relationship it can be inferred that the revival time and the classical period for a particle evolving in a potential constructed from $\mathcal{W}(x) = x^3$ will have some sort of state dependence. To demonstrate this I consider a Fermi-gas quenched from $V^{(1)} \to V^{(2)}$ at $T = 0$ for different particle numbers as seen in Fig. 4.2. One can see that the survival probability contains a clear beating pattern and also revivals of the initial state [148, 149]. While the shape of this beating is consistent throughout all quenches, increasing the number of particles decreases the period of the beating pattern. At finite temperature one can see that the structure of the survival probability changes dramatically and no more revivals occur. Furthermore, for larger particle numbers the survival probability goes to zero quickly, indicating that signs of the orthogonality catastrophe can also be found in SUSY quenches.

4.6.2 $\mathcal{W}(x) = A\,\mathbf{tanh}(x/a)$

Another interesting superpotential is that of the inverse sech^2 potential. Potentials that incorporate hyperbolic functions have in the past shown to have interesting properties [63] with, for example, the Pöschl-Teller potential and its partner potentials, possessing reflectionless states [65]. Potentials of this nature are also ingrained with relationships between one another using point canonical transformations and projections [64]. To develop a reasoning for choosing this potential, consider the inverse sech^2 potential of the form

$$V(x) = -\frac{\hbar^2\nu(\nu+1)}{2ma^2}\text{sech}^2\left(x/a\right), \tag{4.38}$$

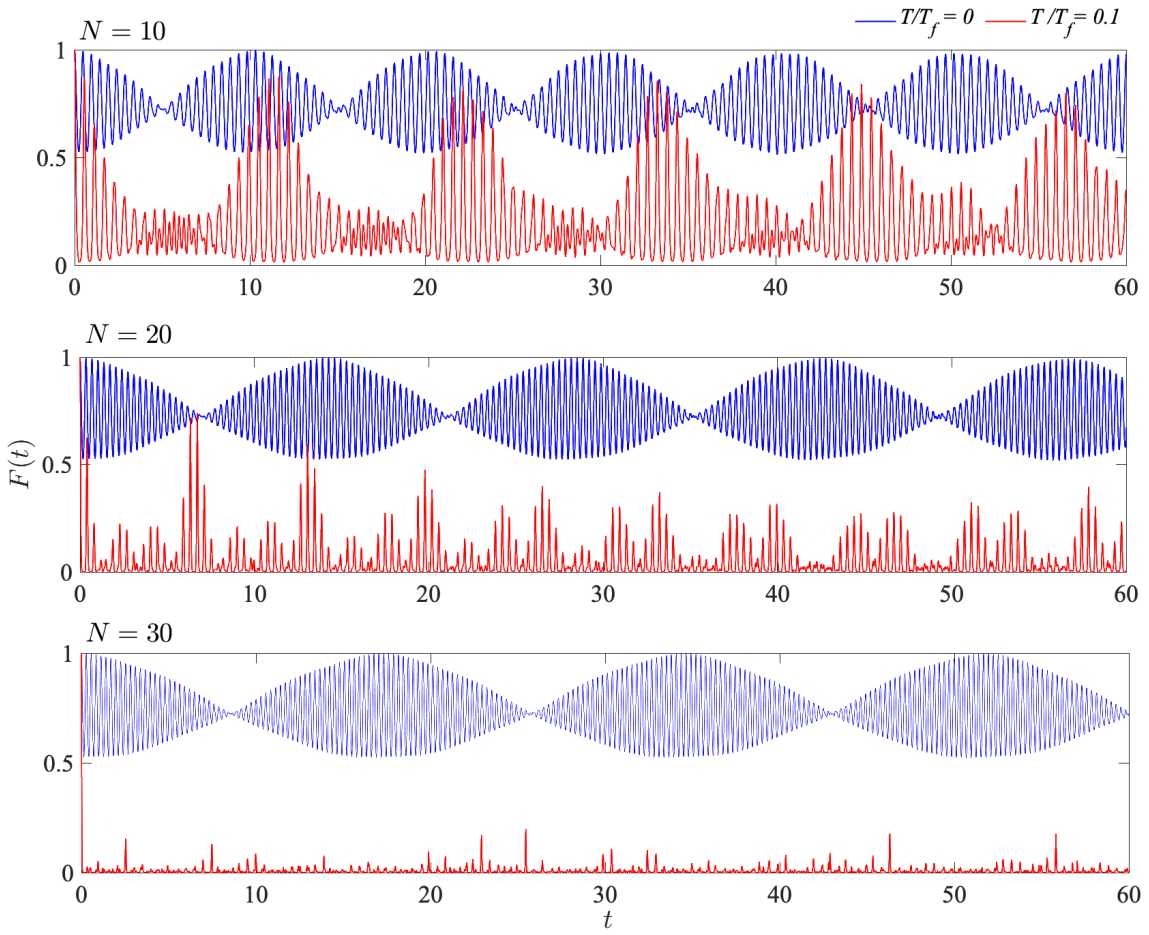

Figure 4.2: Survival probability for a quench between partner potentials constructed using a superpotential $\mathcal{W}(x) = x^3$. The particle numbers for each panel are N=10 (top), N=20 (middle) and N=30 (bottom), for temperatures at $T = 0$ (blue) and $T = T_f/10$ (red).

where the parameters a and ν determine the width of the potential and the depth respectively. The eigenspectrum is similar to the infinite box in that it has an n^2 dependence

$$E_n = -\frac{\hbar^2(\nu - n)^2}{2ma^2} \tag{4.39}$$

for $n = 1, 2, 3..., \nu$ [150]. However, compared to the ISW, here the largest energy gap is between the ground state and the first excited state. The sech^2 potential also only contains a finite number of states, where the highest excited state occurs when $n = \nu$. This imposes some constraints on a SUSY quench for such a potential, limiting the number of fermions that can be used for a given depth. It also puts a hard limit on the number of excitations that can occur from the quench dynamics. Nevertheless we can still find that the revival time of a state in the inverse sech^2 is also independent of

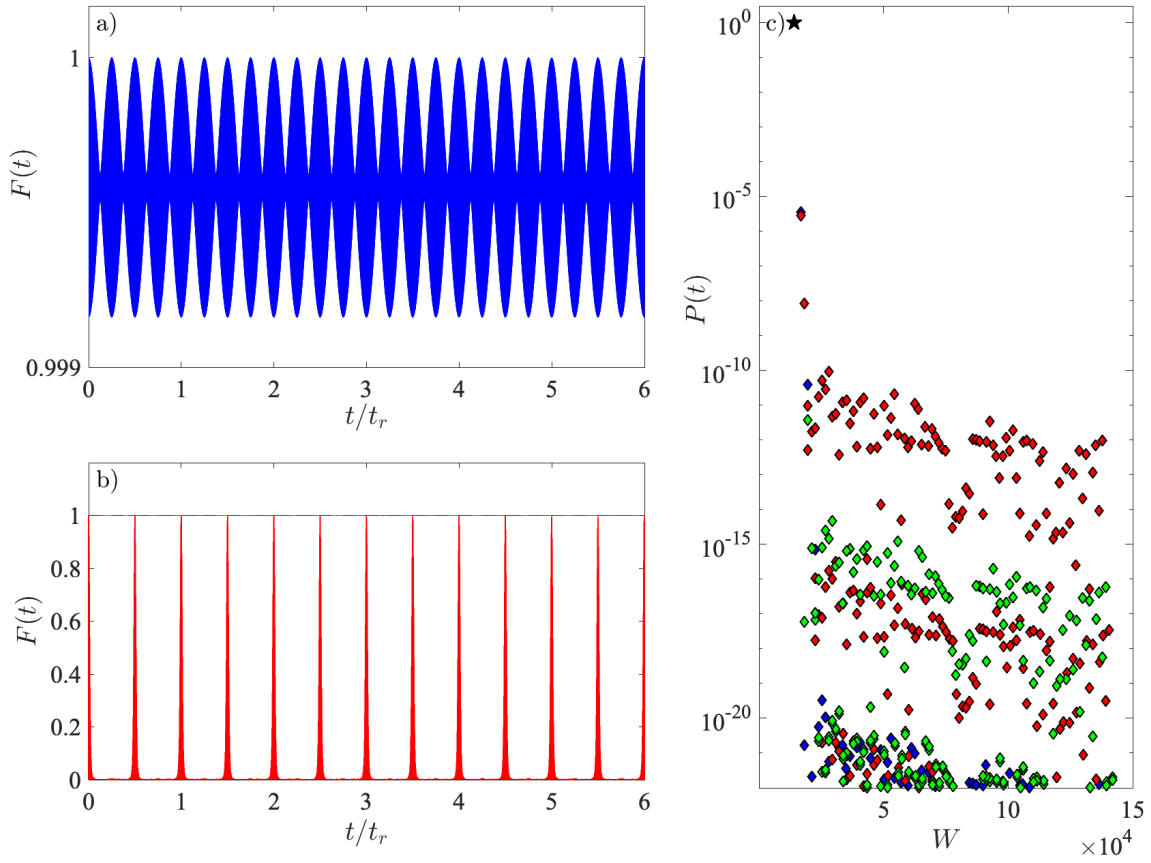

Figure 4.3: Survival probability of a quench using $\mathcal{W}(x) = A\tanh(x/a)$ at $T = 0$ (a) and $T/T_F = 0.25$ (b). (c) The WPD distribution at $T = 0$

the state, with a revival time calculated from the energy in Eq. (4.39) as

$$t_r = \frac{4\pi m a^2}{\hbar^2} \,. \tag{4.40}$$

Rearranging the equation for the revival time and saying $\frac{\hbar^2}{2ma^2} = \frac{2\pi}{t_r}$ I can derive an expression similar to the ISW in Eqs (4.34) and (4.33). For revivals at $t = t_r/4$ one can find a difference in phase of $\pi \mod 2\pi$ for unlike phases (differences between even and odd or odd and even wavefunctions) or $0 \mod 2\pi$ for like phases (differences between even and even or odd and odd wavefunctions). At $t = t_r/2$ on the other hand all phase differences are simply $0 \mod 2\pi$. In my work for the ISW supersymmetric quench I noted that revivals in a many-body system post quench occur at finite temperature if the phases of the overlaps at $T = 0$ are at $0 \mod 2\pi$. With similar results emerging from the inverse sech^2 potential quench we would also expect to find revival retention.

For simplicity we consider arbitrary constants in the construction of our two partner

potentials. For an inverse sech^2 potential the corresponding superpotential is

$$\mathcal{W} = A \tanh(x/a) \,, \tag{4.41}$$

where $a = 1$ modulates the trap width and A is the trap depth large enough to hold a small system of fermions. The potentials resulting from this superpotential are

$$V^{(1)} = (1 - \text{sech}^2(x/a))A^2 - \frac{A}{a\sqrt{2}} \text{sech}^2(x/a) \tag{4.42}$$

$$V^{(2)} = (1 - \text{sech}^2(x/a))A^2 + \frac{A}{a\sqrt{2}} \text{sech}^2(x/a) \,. \tag{4.43}$$

In Figure 4.3 I show the results obtained by quenching a Fermi gas of five particles between $V^{(1)}$ and $V^{(2)}$. In panel a) when $T = 0$ the survival probability remains high with revivals appearing at $t = t_r/4$. Not only that when finite temperature is introduced half of the revivals also survive for temperatures of $T = T_f/4$. The retention of revivals is consistent with the analysis for the ISW and shows that the retention of revivals are purely an effect dictated by the structure of the eigenspectrum. The WPD shown in panel c) shows that the ground state transition (marked by a black star) is the most probable excitation after a quench.

4.7 Conclusion

In this Chapter I have laid out the tools we have used for calculating the nonequilibirum dynamics in a non-interacting gas quenched between two supersymmetric potentials. In the publication presented I used the ISW as an example to highlight the advantages of using a degenerate eigenspectra, as intrinsic properties such as the classical period and the revival time of a wavefunction carry over between potentials. I also present an analytical derivation of the survival probability in the picture of supersymmetric quenches for any family of potentials which present a hierarchy developed using the factorization methods of supersymmetry. I have shown that quenching between SUSY potentials offers a unique advantage in some cases. Specific to the ISW, high survival probabilities can be achieved at zero temperature for both SUSY quenching and generic changes in the length of the box itself. However in the finite temperature regime the SUSY ISW quenches retain their periods of high revivals where as the infinite box does not. This is due to the retention of the original eigenspectra of the ISW during the quenching process. By observing the phase of the overlaps during each of the revivals we can see that overlaps at $0 \mod 2\pi$ are unaffected by changes in temperature, where as for all other phases of the overlaps there is a shift away from the complex unit circle.

Using different SUSY quenches it can be shown that this is an effect that is directly dependent on the eigenspectrum of the quenching potentials. When this model is applied to potentials with a superpotential such as $\mathcal{W}(x) = x^3$ it can be approximated that the revival time is now state dependent. This can be seen in Figure 4.2, where for different values of particle numbers the survival probability exhibits a beating pattern and regularly approaches one. At finite temperature this beating pattern is destroyed, despite both systems still having the same eigenspectrum. On the other hand, when the

quench is between potentials related to the superpotential ($\mathcal{W}(x) = A\tanh(x/a)$), the revivals are retained at finite temperature, see Figure 4.3. This is a result of the sech potential also having n^2 dependence on the quantum number for the eigenspectrum and as a result the revival time does not have any state dependence. For this reason we can say that the revival retention in SUSY quenches is an effect derived from the structure of the eigenspectrum and quenches between certain potentials with the same spectrum can give additional insight into nonequilibrium many-body dynamics.

Chapter 5

Quantum control and quantum speed limits in supersymmetric potentials

5.1 Introduction

While quenching a gas allows one to push a system far away from equilibrium almost instantaneously, it is equally as important to explore the controlled dynamics of a quantum system for the purposes of engineering quantum devices. An important figure of merit for this is the fidelity between the obtained state at the end of the evolution and the desired one, which is given by the overlap between these two wavefunctions. It is worth noting that this is similar to the survival probability discussed in Chapter 4, where the reference wavefunction was instead the initial state of the system. The fidelity therefore serves as an identifier of the likelihood of excitations appearing during a dynamical process, with a quench being the fastest method to induce these quickly [151]. In many cases however excitations are not desired during the evolution, especially in applications for quantum simulation and sensing.

To prevent excitations from being generated in a quantum system the most obvious solution is to change it at a slow enough speed so that it stays in a single eigenstate at all times, i.e. adiabatically. For a system subjected to some perturbation of its Hamiltonian, whether it be a translation [152, 153], a transformation of the functional form of the external potential [154], or a tuning of the interactions in an ultracold gas [155–157], the adiabatic theorem says that so long as the perturbation acts slowly on a system, the system will remain in an instantaneous eigenstate of the Hamiltonian [158, 159]. While such a level of high fidelity is achievable and has been demonstrated, it is equally as important to search for protocols that achieve the same high level over the shortest time interval possible. Without such protocols, advances in quantum technologies might be hampered by the effects of accumulating external noise and decoherence [5]. Luckily, methods which *speed up* the dynamics whilst inhibiting excitations are studied extensively, the most common of which being Shortcuts to Adiabaticity (STAs). Before being named STA, the idea of fast optimal population control of a quantum system was proposed by Demirplak and Rice [160], expanded upon by Berry [161], and in 2010 Chen *et al.* coined the term STA for the first time [162]. Since then many STA protocols have been studied and have been applied to a wide range of systems [163].

Such techniques are also important in the context of quantum heat engines, where fast adiabatic dynamics is important in cyclic process of expansion and compression of a system [164–166]. In the following sections I will go into detail on the different quantities and functions used to characterize STAs, such as the quantum speed limit, counterdiabatic driving and the associated costs.

5.2 Quantum Speed Limits

Unfortunately, *there is no such thing as a free lunch* [167] and while achieving a high fidelity in short amounts of time is possible, there is a natural fundamental limit on the speed with which quantum systems can evolve. The quantum speed limit (QSL) is a bound on the length of time over which a pure initial state can evolve into a final target state. Mandelstam and Tamm realised that the energy time relationship derived from the Heisenberg uncertainty principle

$$\Delta E \Delta t \geq \hbar \,, \tag{5.1}$$

was actually a description for identifying an intrinsic timescale of quantum dynamics [168]. The derivation for the speed limit starts with the following inequality

$$\Delta H \Delta A \geq \frac{\hbar}{2} \left| \left\langle \frac{\partial A}{\partial t} \right\rangle \right| , \tag{5.2}$$

where ΔH and ΔA are the variances of the Hamiltonian and a chosen observable A. If A is chosen as a projector of an initial state $|\psi(0)\rangle\langle\psi(0)|$, then the inequality can be integrated over time such that

$$\frac{1}{\hbar}\Delta H t \geq \frac{\pi}{2} - \arcsin\sqrt{\langle A \rangle_t}. \tag{5.3}$$

If we consider a final time τ such that the time evolved state is orthogonal to the initial state $\langle\psi(0)|\psi(\tau)\rangle = 0$, then a bound on the minimal time for a quantum system to travel between two orthogonal states is given by

$$t \geq \tau_{QSL} \equiv \frac{\pi}{2}\frac{\hbar}{\Delta H} \,. \tag{5.4}$$

This was the first proposal of a QSL time, τ_{QSL}. Later, Margolus and Levitin proposed an alternative derivation based on the overlap of the time-dependent Schrödinger equation [169]. Consider a time-evolved wavefunction such that the overlap can be written as

$$\langle\psi(0)|\psi(t)\rangle = \nu(t) = \sum_n |c_n|^2 e^{(-iE_n\hbar/t)} \,. \tag{5.5}$$

The real and imaginary parts of the overlap can be separated such that

$$\text{Re}\ \nu(t) = \sum_n |c_n|^2 \cos(E_n t/\hbar) \,. \tag{5.6}$$

Using trigonometric inequalities this real part of the overlap can be written as

$$\text{Re } \nu(t) \geq 1 - \frac{2}{\pi}\frac{\langle H \rangle}{\hbar}t + \frac{2}{\pi}\text{Im } \nu(t) \ . \tag{5.7}$$

Similar to before, a time τ at which the time evolved state and the initial state are orthogonal to each other, $\nu(t) = 0$, is considered. In this case the lower bound for this evolution is described by the average energy $\langle H \rangle$ and is given by

$$t \geq \tau_{QSL} \equiv \frac{\pi}{2}\frac{\hbar}{\langle H \rangle} \ . \tag{5.8}$$

While the two quantities are based on two different properties of the system, both hold true and Levitin and Toffoli [170] later showed that they can be combined to set the fundamental limit on the evolution of a quantum state.

Since then these limits have been studied for a variety of different systems and a comprehensive review of quantum speed limit is given in a recent review by Campbell and Deffner [171]. QSLs have also been derived for non-orthogonal states and for dynamics driven by time-dependent Hamiltonians $H(t)$. To facilitate this a measure to quantify the distance between the initial and target state is required to find the actual speed limit of the system. For this it is common to use the Bures angle $\mathcal{L}$ which is the smallest geometric distance between an initial state at time $t = 0$ and the driven state at $t = \tau$, written as

$$\mathcal{L} = \arccos(|\langle \psi(x,0)|\psi(x,\tau)\rangle|) \ . \tag{5.9}$$

It was shown by Deffner and Lutz [172] that the maximal rate of change of the Bures angle is bounded by

$$\partial_t \mathcal{L} \leq \frac{E}{2\cos(\mathcal{L})\sin(\mathcal{L})}, \tag{5.10}$$

where $E = \langle H(t) \rangle$ is average energy of the time dependent Hamiltonian. Integrating this over time yields the QSL time for the driven dynamics

$$\tau \geq \tau_{QSL} \equiv \frac{\hbar}{2\langle E \rangle_\tau}[\sin(\mathcal{L})]^2, \tag{5.11}$$

where the time averaged energy is

$$\langle E \rangle_\tau = \frac{1}{\tau}\int_0^\tau dt \ \langle H(t) \rangle \ , \tag{5.12}$$

and τ is the duration of the driving. This QSL time is then analogous to the Margolis-Levitin bound for driven systems [172]. Driving protocols for time-dependent Hamiltonians that can work at the speed limit can, for example, be obtained using the techniques known in the field of STAs and will be introduced below.

Studying STAs and QSLs in supersymmetric systems allows one to explore the effect of different Hamiltonians, which all have the same eigenspectrum. In my work I have focused on studying STAs for two different classes of wavefunctions: one is a group of ground state wavefunctions of a hierarchy of supersymmetric Hamiltonians and the

other are a set of energetically degenerate states within the same hierarchy. Since the ground states all have the same functional form, but different energies, and the degenerate states have different functional forms, but the same energy, this approach allows one to distinguish between the effects coming from the distance in Hilbert or in energy space.

5.3 Shortcuts to Adiabaticity

In this section I will focus on STAs and specifically deriving counterdiabatic driving terms. I will motivate the use of counterdiabatic driving starting from Berry's formulation of the counterdiabatic term followed by a derivation of this term using the Jarzynski derivation for an ISW. I will then extend the properties of intertwining the supersymmetric Hamiltonians and include the counterdiabatic driving term.

5.3.1 Counterdiabatic Driving

One way to maintain perfect fidelity for a single-particle state that evolves during a time-interval τ in any time-dependent Hamiltonian is to apply an auxiliary field that can counteract the fluctuations arising from excitations. To facilitate this an additional, counterdiabatic Hamiltonian H_{CD} can be added to the single particle Hamiltonian H_0, which ensures that adiabaticity is maintained [161] so that the overall Hamiltonian looks like $H(t) = H_0(t)+H_{CD}(t)$. To find such a counterdiabatic Hamiltonian, consider the single particle Hamiltonian with instantaneous eigenstates and energies

$$H_0(t)|m(t)\rangle = \mathcal{E}_m(t)|m(t)\rangle \ . \tag{5.13}$$

To obtain adiabaticity, the evolved state can be written using the instantaneous eigenstates as

$$|\psi_m(t)\rangle = e^{i\alpha_m(t)}|m(t)\rangle, \tag{5.14}$$

where the exponential term is the adiabatic phase given by

$$\alpha_m(t) = -\frac{1}{\hbar}\int_0^t dt'\mathcal{E}_m(t') + i\int_0^t dt'\langle m(t')|\partial_{t'}m(t')\rangle \ . \tag{5.15}$$

One can see that a geometric phase is induced by the changing of the instantaneous eigenstates over time as $\langle m(t')|\partial_{t'}m(t')\rangle$.

As the wavefunction evolves over time we note that the wavefunction must follow the instantaneous eigenstates $|m(t)\rangle$. This ensures that there are no transitions over all times for the evolving state,

$$i\hbar\partial_t|\psi_m(t)\rangle = H(t)|\psi_m(t)\rangle \, . \tag{5.16}$$

$H(t)$ can then be constructed using unitary evolution operators such that the operator $U(t)$ is a solution to $i\hbar\partial_t U(t) = H(t)U(t)$, allowing the Hamiltonian to be written as

$$H(t) = i\hbar(\partial_t U(t))U(t) \ . \tag{5.17}$$

By choosing $U(t) = \sum_m e^{i\alpha_m(t)}|m(t)\rangle\langle m(0)|$ and differentiating with respect to time, the time dependent Hamiltonian can be constructed as

$$\begin{aligned} H(t) &= H_0(t) + H_{CD}(t) \\ &= H_0(t) + i\hbar \sum_m (|\partial_t m(t)\rangle\langle m(t)| - \langle m(t)|\partial_t m(t)\rangle |m(t)\rangle\langle m(t)|) \,, \end{aligned} \tag{5.18}$$

where $H_0 = \sum_{m=1}^{N} \mathcal{E}_m(t)|m(t)\rangle\langle m(t)|$. The time-dependent Hamiltonian then effectively nullifies nonadiabtaic excitations such as the geometric phase $\langle \partial_t m(t)|m(t)\rangle = 0$ and ensures that the driven state always follows the instantaneous eigenstate $\psi_m(x,t) = e^{-i\int_0^t \mathcal{E}_m(t')dt'}|m(t)\rangle$, realizing adiabatic dynamics for any value of τ. This reduces the counterdiabatic driving term to [160, 173, 174]

$$H_{CD,m}(t) = i\hbar|\partial_t m(t)\rangle\langle m(t)| \,. \tag{5.19}$$

Over the past couple of years, many counterdiabatic protocols have been developed for different situations with different external potentials [163]. To highlight the use of supersymmetry in counterdiabatic driving we once again choose the infinite square well as our potential.

5.3.2 Scale Invariant Driving, Generating Functions

The generation of the CD term has been generalized by Jarzynski [175] who showed that a generator of adiabatic transport, $\xi(t)$, can be used to obtain the CD term necessary to implement a shortcut. Conveniently, Jarzynski illustrates the construction of this using an expanding ISW potential, similarly to the situation I will discuss in my work. In this section I will therefore present this derivation of the generator of adiabatic transport to understand how the CD term modulates the wavefunction. To start the CD Hamiltonian can be written in the form

$$H(t) = H_0(L(t)) + \dot{L}(t) \cdot \xi(L(t)) \tag{5.20}$$

where $L(t)$ is the time dependent length of the ISW in H_0 and $\xi(t)$ replaces the generalized form of the counterdiabatic term in Eq. (5.18). ξ acts as the generator that converts infinitesimal displacements in space, $L \to L + \delta L$ to displacements in the Hilbert space $|\psi\rangle \to |\psi\rangle + |\delta\psi\rangle$, which when applied to the eigenstates of Hamiltonian $H_0(L(t))$ generates

$$|m(L)\rangle \to \left(1 + \frac{1}{i\hbar}\delta L \cdot \xi\right)|m(L)\rangle = e^{i\delta L A_n}|m(L+\delta L)\rangle, \tag{5.21}$$

where A_n is a phase imparted on a wavefunction [176]. The task now is to find a solution for the generator ξ. In his derivation, Jarzynski compares the aforementioned displacement in Hilbert space to that of a classical example where the displacement takes place in phase space, ($z = [q,p]$). The generator then serves as a converter between the changes of the time dependent parameters (L) and phase space. Over time as the length of the potential increases, the mapping between $H_0(z;L)$ and $H_0(z;L+\delta L)$

can be used in order to construct the generator. Starting with the Hamiltonian for an ISW with walls at $q = 0$ and L

$$H_0(z; L) = \frac{p^2}{2m} + V_{box}(q; L), \tag{5.22}$$

and increasing the length of the box from L to $L(1 + \delta L/L)$, the coordinates in phase space transform linearly

$$q \to q\,(1 + \delta L/L) \quad , \quad p \to p\,(1 + \delta L/L)\,. \tag{5.23}$$

Classically a solution for the generator can be found by taking the change in phase space as

$$\left(\frac{\delta L}{L}q, -\frac{\delta L}{L}p\right) \equiv \delta z = \delta L\{z, \xi\}, \tag{5.24}$$

where $\{\cdot, \cdot\}$ are the Poisson brackets. Solving for this transformation produces the equations $p/L = \partial\xi/\partial q$ and $q/L = \partial\xi/\partial p$. The solution for the generator is then of the form $\xi = \frac{qp}{L}$ and from Eq. (5.20) the full Hamiltonian reads

$$H(z; L) = H_0(z; L) + \frac{\dot{L}}{L}qp \tag{5.25}$$

By finding a classical solution to the generator ξ a quantum solution can be motivated. Since q and p do not commute, one instead arrives to the solution

$$\xi = \frac{qp + pq}{2L}. \tag{5.26}$$

It so happens that this can be applied to the infinite box and the displacement condition Eq. (5.21) producing the wavefunction

$$\left(1 + \frac{1}{i\hbar}\delta L\,\xi\right)\psi(q, L) = \sqrt{\frac{2}{L + \delta L}}\sin\left(\frac{n\pi q}{L + \delta L}\right). \tag{5.27}$$

Plugging the parameters of the length of the box and the generator into Eq. (5.20), the full Hamiltonain can then be written as

$$H_0(z; L) = \frac{p^2}{2m} + V_{box}(q; L) + \frac{\dot{L}}{2L}\,(qp + pq)\,, \tag{5.28}$$

where the counterdiabatic modulation of the Hamiltonian is proportional to $\frac{\dot{L}(t)}{L(t)}$. Modulations such as this have been identified in a large class of potentials found in [163], even identifying that the these hold true for supersymmertic potentials as well.

5.3.3 Driving of SUSY partner Potentials

Now that the counterdiabatic term is defined for the ISW we need a way to modulate the length of the box between $t = \{0, \tau\}$. In previous studies the most suitable modulation

of the length of the box has been found to be a smooth function of the form [174, 177]

$$L(t) = L_i + (L_f - L_i)\left(\frac{t}{\tau}\right)^3 \left(10 - 15\frac{t}{\tau} + 6\frac{t^2}{\tau^2}\right) , \tag{5.29}$$

for which the following boundary conditions are fulfilled

$$L(0) = L_i \quad , \quad L(\tau) = L_f \tag{5.30}$$

$$\dot{L}(0) = \dot{L}(\tau) = 0 . \tag{5.31}$$

These boundary conditions ensure that the time-dependent Hamiltonian at the start and the end of the ramping is equal to the single particle Hamiltonians, i.e. $H(0) = H_0(0)$ and $H(\tau) = H_0(\tau)$, see Eq. (5.28), and therefore the state is a stationary eigenstate. For other potentials and perturbations to a Hamiltonian, parameters of the Hamiltonian can be subjected to different ramps which ultimately optimize the transport of a dynamic system [178, 179]. The next task is now to incorporate the time-dependent length of the box into the SUSY description of the ISW.

Typically for STAs in an ISW, the length of the box is modulated using Eq. 5.29. This can be done either symmetrically around the center of the potential or by allowing only one wall to move [105]. In my work I focus on a symmetric expansion of the potential around the center of the potential, similar to the situation of the quenches discussed in Chapter 4. During the expansion of the ISW the instantaneous ground state is therefore time dependent such that

$$\psi_1(x,t) = \sqrt{\frac{2}{L(t)}}\cos\left(\frac{x\pi}{L(t)}\right) . \tag{5.32}$$

As a consequence of this the calculation of the superpotential in Eq. (2.6) also becomes time dependent, as well as the SUSY operators. Using Eq. (2.6), the superpotential can be calculated at every time step producing

$$\mathcal{W}^{(\alpha)}(x,t) = \alpha\frac{\hbar\pi}{\sqrt{2m}L(t)}\tan\left(\frac{x\pi}{L(t)}\right) . \tag{5.33}$$

The resulting potentials are then written as

$$V^{(\alpha)}(x,t) = \mathcal{W}^{(\alpha)}(x,t)^2 - \frac{\hbar\mathcal{W}^{(\alpha)}(x,t)'}{\sqrt{2m}}$$

$$V^{(\alpha+1)}(x,t) = \mathcal{W}^{(\alpha)}(x,t)^2 + \frac{\hbar\mathcal{W}^{(\alpha)}(x,t)'}{\sqrt{2m}} .$$

This preserves one of the main features of SUSY potentials: using a time dependent superpotential ensures that two potentials will expand at a rate at which degeneracy between all potentials is maintained throughout the ramping. The intertwining properties are also preserved during the ramping as the time dependent operators $A^{(\alpha)}(x,t)$ and $A^{(\alpha)\dagger}(x,t)$ can act on the wavefunctions for all of t. For these reasons its also

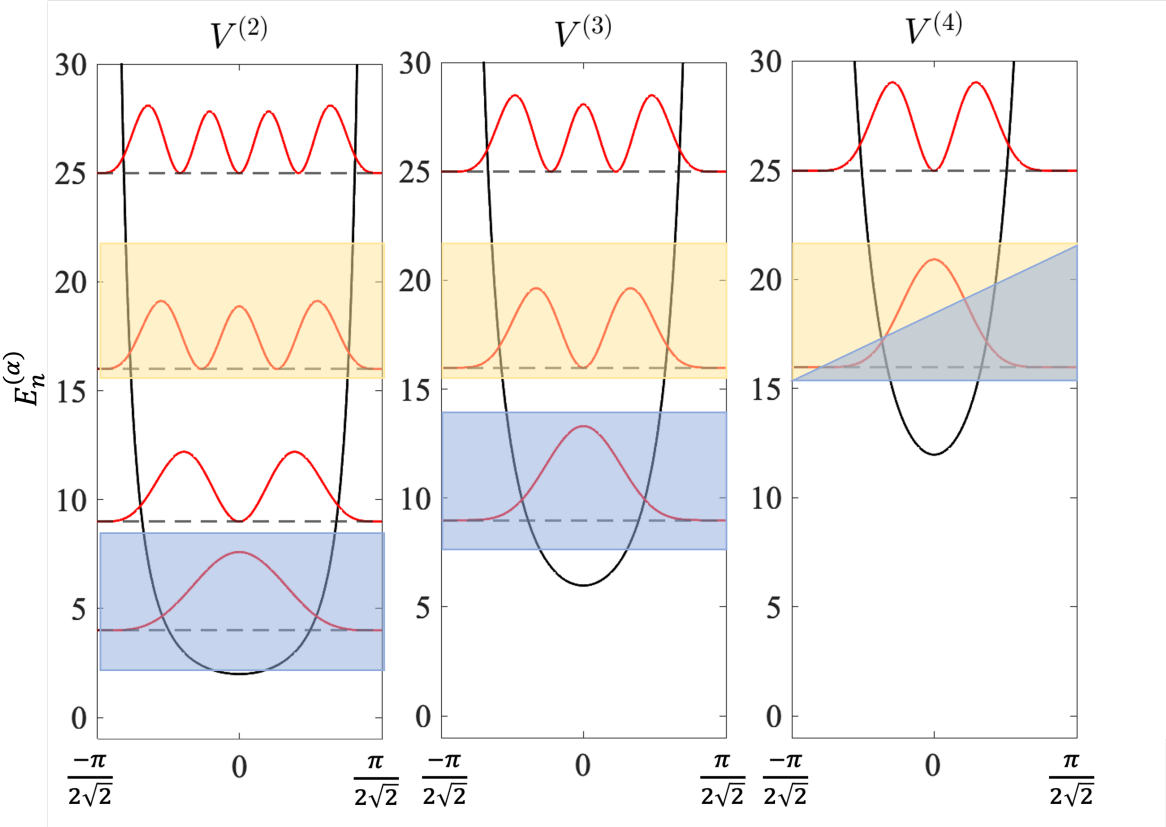

Figure 5.1: The first three partner potentials of the infinite square plotted with the probability density of their eigenfunctions. Blue: Set one, highlighting differences in the ground states. Yellow: Set two, highlighting differences in iso-spectral wavefunctions. In this schematic I have set $\hbar = m = 1$ so that $E_n = (n + \alpha - 1)^2$.

important to define the energy in terms the order of the potential α and the principle quantum number of the state n. The energy spectrum for any potential in a SUSY hierarchy of the ISW can then be written as

$$\mathcal{E}_n^{(\alpha)}(t) = \frac{(n + \alpha - 1)^2 \pi^2 \hbar^2}{2mL(t)^2} \,. \tag{5.34}$$

The degeneracy from SUSY QM still holds such that $\mathcal{E}_n^{(\alpha)} = \mathcal{E}_{n-1}^{(\alpha+1)}$.

In this work I want to compare the QSL time, fidelity and the cost of two different sets of wavefunctions that are related in to each other in either energy, which is the isospectral case, or in shape, which is a set of ground state wavefunctions. For this reason I have chosen the three neighbouring partner potentials, $\alpha = 2, 3, 4$, and have used their ground states as one set of wavefunctions $(|\psi_1^{(4)}\rangle, |\psi_1^{(3)}\rangle, |\psi_1^{(2)}\rangle)$ with energies of $\mathcal{E}^{(\alpha)} = \frac{\alpha^2\pi^2\hbar^2}{2mL(t)^2}$ (labelled in blue in Figure 5.1), and the three states isospectral with one another $(|\psi_1^{(4)}\rangle, |\psi_2^{(3)}\rangle, |\psi_3^{(2)}\rangle)$, with energies of $\mathcal{E}^{(\alpha)} = \frac{16\pi^2\hbar^2}{2mL(t)^2}$ (labelled in yellow in Figure 5.1). This will allow me to explore the QSL time under two different constraints. The set of ground state wavefunctions have almost identical Bures angles (in Eq. (5.9)), which is not the case for the isospectral wavefunctions. This means that the dominating

contribution to the QSL time come from the time averaged energy difference at the start and end of the ramp

$$\Delta\mathcal{E}_1^{(\alpha)} = \frac{\alpha^2\pi^2\hbar^2}{2m}\left(\frac{1}{L_i^2} - \frac{1}{L_f^2}\right) , \tag{5.35}$$

which can be seen to increase with α^2. This differs from the isospectral case, where the degeneracy means that the energetics are similar, however the Bures angles differ significantly as more nodes are added to the wavefunction with increasing α. In the publication I show that, despite the large degeneracies between the different settings, the average energies required for short ramp times differ greatly and are due to either the Bures angle or the differences in spectrum, but for larger ramp times at the adiabatic limit the average energies become comparable to each other as

$$\langle E_n\rangle_{AD} = \int_0^\tau dt\ \mathcal{E}_n^{(\alpha)}(t) . \tag{5.36}$$

It is therefore interesting to explore the cost of driving the system, which requires first to study the intertwining properties of the counterdiabatic driving terms.

5.4 Intertwining of the Counterdiabatic Term

In Eq. (2.11) the intertwining relationship using the creation and annihilation operators between sets of partner Hamiltonians created using factorization techniques was given. As a result of this, the degeneracy between the eigenspectra could be derived, which allowed wavefunction transformations between the different Hilbert spaces. When a hierarchy of supersymmetric Hamiltonians is considered, wavefunction transformations can be facilitated recursively, as long as an annihilation operator does not act on a ground state wavefunction. Consequently, the properties and values that are dependent on the eigenspectra transfer between Hamiltonians. This was explored in Chapter 4 where I took advantage of the fact that the revival time for a wavefunction in a supersymmetric ISW hierarchy is dependent on the eigenspectrum of the original Hamiltonian. In this section we will explore an extension of these intertwining properties on the counterdiabatic driving term.

To start, recall that for all ground states the general form of the ground state wavefunction in the ISW is

$$\psi_1^{(\alpha)} = \frac{1}{\sqrt{L(t)}}\left[\frac{\sqrt{\pi}\Gamma(\alpha+1)}{\Gamma(\alpha+\frac{1}{2})}\right]^{\frac{1}{2}}\cos\left(\frac{x\pi}{L(t)}\right)^\alpha , \tag{5.37}$$

where α identifies the order of the potential. Following this the time derivative of the wavefunction is

$$\partial_t\psi_1^{(\alpha)} = \psi_1^{(\alpha)}\left[-\frac{1}{2} + \frac{\pi x\alpha}{L(t)}\tan\left(\frac{\pi x}{L(t)}\right)\right]\frac{\dot{L}(t)}{L(t)} . \tag{5.38}$$

Inserting these two expressions into the definition of the counterdiabatic term, one can explicitly see that the modulation of the length, $\dot{L}(t)/L(t)$, calculated in Eq. (5.28), is present for all groundstates of the supersymmetric ISW hierarchy [163, 175].

For the isospectral wavefunctions, the counterdiabatic terms do in fact have an intertwining relationship. To see this, recall that for an isospectral set of wavefunctions the transformation between two different Hilbert spaces requires the use of a specific SUSY operator, which has to be normalized using the energy difference of the ground state of the lower potential and the energy of the transformed wavefunction, see Eqs. (2.16) and (2.15). The counterdiabatic term can therefore be written in terms of its partner term by rewriting the wavefunctions using the aforementioned transformations. Using $|\psi_n^{(\alpha+1)}\rangle$ as the instantaneous eigenstate of $H^{(\alpha+1)}$, the counterdiabatic term can be written as

$$\begin{aligned} H_{CD,n}^{(\alpha+1)} =& i\hbar\partial_t|\psi_n^{(\alpha+1)}\rangle\langle\psi_n^{(\alpha+1)}| \\ =& \frac{i\hbar}{\Delta\mathcal{E}_{n+1}^{(\alpha)}}\partial_t\left(A^{(\alpha)}|\psi_{n+1}^{(\alpha)}\rangle\right)\langle\psi_{n+1}^{(\alpha)}|A^{(\alpha)\dagger}\,. \end{aligned} \tag{5.39}$$

Using the quotient rule, the time derivative can be expanded as the operator $A^{(\alpha)}(t)$ is also time-dependent, giving us $\partial_t\left(A^{(\alpha)}|\psi_{n+1}^{(\alpha)}\rangle\right) = \partial_t\left(A^{(\alpha)}\right)|\psi_{n+1}^{(\alpha)}\rangle + A^{(\alpha)}\left(|\partial_t\psi_{n+1}^{(\alpha)}\rangle\right)$. This leaves the final equation for the adjacent CD term as

$$H_{CD,n}^{(\alpha+1)} = \frac{1}{\Delta\mathcal{E}_{n+1}^{(\alpha)}}A^{(\alpha)}H_{CD,n+1}^{(\alpha)}A^{(\alpha)\dagger} + \frac{i\hbar}{\Delta\mathcal{E}_{n+1}^{(\alpha)}}(\partial_t A^{(\alpha)})|\psi_{n+1}^{(\alpha)}\rangle\langle\psi_{n+1}^{(\alpha)}|A^{(\alpha)\dagger}\,, \tag{5.40}$$

where $H_{CD,n+1}^{(\alpha)} = i\hbar|\partial_t\psi_{n+1}^{(\alpha)}\rangle\langle\psi_{n+1}^{(\alpha)}|$ is the CD Hamiltonian for the state $|\psi_{n+1}^{(\alpha)}\rangle$ and the second term arises due to the time-dependence of the supersymmetric operator $A^{(\alpha)}$. Alternatively, in the opposite direction (from α to $\alpha+1$), the counterdiabatic terms can be related in a similar way

$$H_{CD,n+1}^{(\alpha)} = \frac{1}{\Delta\mathcal{E}_{n}^{(\alpha)}}A^{(\alpha)\dagger}H_{CD,n}^{(\alpha+1)}A^{(\alpha)} + \frac{i\hbar}{\Delta\mathcal{E}_{n}^{(\alpha)}}(\partial_t A^{(\alpha)\dagger})|\psi_{n}^{(\alpha+1)}\rangle\langle\psi_{n}^{(\alpha+1)}|A^{(\alpha)}\,, \tag{5.41}$$

While this expression for the intertwining relations of the CD Hamiltonian is not as simple as for the single particle Hamiltonian alone, it shows that the CD term for the next higher supersymmetric Hamiltonian can be constructed with only knowledge of the adjacent Hamiltonians and its eigenstates [22]. This has an effect on different values associated with the counterdiabatic term, in particular to the cost of driving a system.

5.4.1 Cost to Counterdiabatic Driving

Let us now look at the relationship between the QSL time and the energetic cost of the counterdiabatic term [167]. The cost is defined as the energy required to achieve adiabatic dynamics of a state for a specific change to a potential, in our case this is an expansion stroke. A common way to quantify this is given by the trace norm of the counterdiabatic driving term $C_n^{(\alpha)} = \int_0^\tau dt||H_{\mathrm{CD,n}}^{(\alpha)}||_{\mathrm{tr}}$ [180] where the integrand can be

written in terms of the time derivative of the instantaneous eigenstates as

$$\partial_t C_n^{(\alpha)} = \sqrt{\langle \partial_t \psi_n^{(\alpha)} | \partial_t \psi_n^{(\alpha)} \rangle} \, . \tag{5.42}$$

From our example of the ISW, since the eigenstates of the full hierarchy of the supersymmetric Hamiltonians related can be written in terms of Chebyshev polynomials of the second kind, it can be exactly evaluated. However these general expressions can become unwieldy for excited states in higher order Hamiltonians very quickly. Thanks to the analysis of the ISW by Gutierrez *et al.* [60], we can write the ground state and the first excited state in a much simpler general form. This will assist us here to illustrate the effect of the intertwining of the counterdiabatic term due to the associated intertwining of the ground state and first excited state of $H^{(\alpha)}$ and $H^{(\alpha-1)}$ respectively. Using the time derivative of the generalized ground state for a $H^{(\alpha)}$, the cost of driving the system can be written as

$$\partial_t C_1^{(\alpha)} = \frac{\dot{L}(t)}{L(t)} \left[-\frac{1}{4} + \int_{-L(t)/2}^{L(t)/2} \psi_1^{(\alpha)} \psi_1^{(\alpha)*} \left(\frac{\pi x \alpha}{L(t)} \tan\left(\frac{x\pi}{L(t)} \right) \right)^2 dx \right]^{\frac{1}{2}} , \tag{5.43}$$

where it is worth noting that the leading term is independent of α, while the integral is order dependent.

Moving one order down from from $\psi_1^{(\alpha)}$ to $\psi_2^{(\alpha-1)}$, we want to find the CD term for the first excited state of the Hamiltonian $H^{(\alpha-1)}$. From our derivation of the CD term in Eq. (5.41) we can expect to find some relationship with the cost $\partial_t C_1^{(\alpha)}$. To start we write the generalized form of the first excited state for all potentials and its time derivative as we did for the ground state

$$\psi_2^{(\alpha)} = \frac{1}{\sqrt{L(t)}} \left[\frac{2\sqrt{\pi}\Gamma(\alpha+2)}{\Gamma(\alpha+\frac{1}{2})} \right]^{\frac{1}{2}} \sin\left(\frac{x\pi}{L(t)} \right) \cos\left(\frac{x\pi}{L(t)} \right)^{\alpha}, \tag{5.44}$$

$$\partial_t \psi_2^{(\alpha)} = \psi_2^{(\alpha)} \left[-\frac{1}{2} - \frac{\pi x}{L(t)} \tan^{-1}\left(\frac{x\pi}{L} \right) + \frac{x\pi\alpha}{L(t)} \tan\left(\frac{x\pi}{L} \right) \right] \frac{\dot{L}(t)}{L(t)}, \tag{5.45}$$

Once again, similar to the ground state cost in Eq (5.43) we can calculate the integral of the time derivative overlap. With some rearranging of the integrals we find that the cost of the first excited state of the ISW can be written in terms of the ground state of the adjacent potential,

$$\partial_t C_2^{(\alpha-1)} = \frac{\dot{L}(t)}{L(t)} \left[-\frac{1}{4} + (2\alpha - 1) \int_{-L(t)/2}^{L(t)/2} \psi_1^{(\alpha)*} \psi_1^{(\alpha)} \left(\frac{x\pi}{L(t)} \right)^2 \right.$$
$$\left. \times \left(1 + (1-\alpha) \tan\left(\frac{x\pi}{L(t)} \right)^2 \right)^2 dx \right]^{\frac{1}{2}} . \tag{5.46}$$

Comparing the equations of the two costs we notice a few similarities. To start the cost has a dependence of the length $\frac{\dot{L}(t)}{L(t)}$ which is expected for all states. The leading term

for both is again not dependent on α. Furthermore, the ingredients for the construction of the ground state cost are also present with the addition of other terms.

We can further confirm the relationship of the costs by calculating the average cost of the system $\langle \partial_t C_n^{(\alpha)} \rangle_\tau = \frac{1}{\tau} \int_0^\tau \partial_t C_n^{(\alpha)}$ for each set of eigenstates, shown in Figure 3. of the publication [2]. We can see how the analytical equations of the cost correspond to one another for both the general ground state case in Eq. (5.43) and for an isospectral counterpart. For the ground states, there is very little difference between the costs as the integral for the cost is only dependent on the order of the potential α. That being said we can still see that the lowest cost to drive the system is the ground state of potential $\alpha = 4$. The isospectral case however shows a clear difference in the average cost of driving a system whilst maintaining the same trend of converging for longer times. Comparing the average cost of $\psi_1^{(4)}$ to $\psi_2^{(3)}$ as an example, the analytical cost of driving tells us that the cost of $\psi_2^{(3)}$ will include the cost of the integrand of $\psi_1^{(4)}$ with some additional terms added to it as calculated above. This goes one step further between $\psi_2^{(3)}$ and $\psi_3^{(2)}$ as the amount of terms added to the cost increases.

This is an important result since the cost of driving the system can be incorporated into the QSL time for a given quantum state. Once the cost is incorporated the time averaged energy then becomes a summation of the instantaneous energy with the associated cost [167], written as

$$\tau_{QSL} = \frac{\hbar\tau[\sin(\mathcal{L}_n^{(\alpha)})]^2}{2\int_0^\tau dt\sqrt{\mathcal{E}_n^2 + (\partial_t C_n^{(\alpha)})^2}} \,. \tag{5.47}$$

From the comparison of the ground states, the cost to drive the system is just as similar as the Bures angle, and therefore the difference in the instantaneous energy ultimately affects the varying differences in the QSL time. Conversely in the isospectral case, the instantaneous energy does not vary between all three states due to the implementation of the expansion through the tuning of the superpotential. For this reason the cost and the Bures angle have the greatest affect on the QSL time.

5.5 Publication

The results of Chapter 5 are published as:

Christopher Campbell, Jing Li, Thomas Busch and Thomás Fogarty
Quantum control and quantum speed limits in supersymmetric potentials
New J. Phys. **24**, 095001 (2022) [2]

I conducted all numerical simulations and analytical calculations related to the fidelity, cost, quantum speed limit and energy functional. I also derived the analytical expressions for the extended intertwining properties of the counterdiabatic driving terms specific to the infinite square well. I wrote the first draft of the paper and all other authors contributed to the discussions, interpretation of results, suggestions of improvements toward presentation of the analytical results and the final production of the material published.

5.6 Remarks

In Chapter 4 I quenched a Fermi gas prepared in an ISW to one of its partner potentials, while in this Chapter I have considered an STA in one superpotential of the ISW. The next step would to incorporate the two projects to implement a shortcut of the ISW, or a different partner potential, to a higher order potential, i.e driving from from $V^{(\alpha)}(x, t = 0)$ to $V^{(\alpha+1)}(x, t = t_f)$. Theoretically this is easy to implement between partner potentials as they use the same SUSY operators. Recall that for the construction of the Hamiltonians $H^{(1)}$ and $H^{(2)}$ in Chapter 2, the main difference between the Hamiltonians can be found in the expression for the potentials, specifically

$$V^{(1)}(x) = \mathcal{W}^{(1)}(x)^2 - \frac{\mathcal{W}^{(1)}(x)'}{\sqrt{2}}, \tag{5.48}$$

$$V^{(2)}(x) = \mathcal{W}^{(1)}(x)^2 + \frac{\mathcal{W}^{(1)}(x)'}{\sqrt{2}} \ . \tag{5.49}$$

Its clear from the two expressions above that the two potentials differ by $2\frac{\mathcal{W}^{(1)}(x)'}{\sqrt{2}}$. This can be generalized however for any set of partner Hamiltonians α and $(\alpha+1)$. Because of this difference we can use a time-dependent parameter which gradually changes the potential between $V^{(\alpha)}$ and $V^{(\alpha+1)}$ and which can be optimized using concepts from shortcuts to adiabaticity. The difference between SUSY partner potentials is dictated by the spatial derivative of the superpotential. While a physical interpretation of this is not known theoretically the following time-dependent potential can be written as

$$V(x, t) = \mathcal{W}(x)^2 + \beta(t)\frac{1}{\sqrt{2}}\frac{d}{dx}\mathcal{W}(x), \tag{5.50}$$

where β is in the range of $\beta \in [-1, 1]$. While the change in energy can be found for the system during the ramping the wavefunctions in between the two partner potentials are not known between $-1 < \beta < 1$. To remedy this for the ISW partner potentials as an example, one can start with the initial and final states of the potentials and a variational ansatz can be engineered in a way that follows the same ramping as the potentials [181–183]. For intermediate times between the initial and final SUSY potentials the following ansatz can be used

$$\tilde{\psi}(x, t) = \mathcal{N}\left[\left(\frac{1}{2} - \frac{\beta(t)}{2}\right)\psi(x, 0) + \left(\frac{1}{2} + \frac{\beta(t)}{2}\right)\psi(x, \tau)\right] \tag{5.51}$$

where $\mathcal{N}$ is a normalization constant, $\psi(x, 0) = \psi_n^{(\alpha)}$ and $\psi(x, \tau) = \psi_{n-1}^{(\alpha+1)}$. This ansatz is then an appropriate place to start to derive the shortcut between partner potentials using inverse engineering [183]. Further extensions to controlled SUSY dynamics can also be made using optimal control techniques [184] which could realize robust shortcuts to higher order SUSY potentials.

5.7 Conclusion

In this work I have used the supersymmetric partner potentials as a platform to study STA protocols using scale-invariant driving. This is achieved by implementing a ramp of the length of the box via the superpotentials, ensuring that the spectral degeneracy is maintained during the expansion. The degenerate eigenspectra between partner potentials allow for the calculations of different values such as the fidelity, QSL time and cost of driving different sets of eigenstates to be compared. For example, by using eigenstates from supersymmetric partner potentials, different values used to calculate the QSL time such as the Bures angle and the average energy can be constrained depending on the states used. In the publication I have used the ISW as an example and I have compared these values for two sets of eigenstates. One set consists of only the ground states of three adjacent potentials and the other contains three eigenstates adjacent to each other which have the same energy. In the first set of eigenstates it can be seen that the Bures angle is loosely constrained and as a result the average energy of the system ultimately determines the QSL time. In the isospectral case, the instantaneous energy of the eigenstates are constant which constrains the average energy at the adiabatic limit. As a consequence the Bures angle directly affects the value in which QSL time converges.

In the next step I considered counterdiabatic driving of the Hamiltonian. By including the CD term we have to consider the cost to drive a system to perfect fidelity in our calculations, changing the QSL time which is now calculated using a sum of the instantaneous energies and the cost rather than the average energy of the system. When calculating the cost for the ISW and its partner potentials, simplifications and generalizations can be made for both sets of wavefunctions. For the cost associated with the ground state, due to the general formula of the ISW ground state [60], we find that the cost is dependent on α with all other parameters remaining the same. By calculating the average cost we can see that the difference between higher order potentials is marginal, echoing that the only difference in the QSL time is dependent on the energy difference between the initial and target states. For the isospectral case on the other hand, intertwining relationships can be exploited and we find that the cost of driving can be written in terms of adjacent wavefunctions. As an example I have analytically calculated the cost of driving between the first excited state of one potential and found that this can be written in terms of the ground state that is isopectral to the first excited. I have also found that the cost of driving is simply the cost of driving the ground state with the addition of other integrals which can still be calculated only from the knowledge of the wavefunctions of the partner potential. The result is reinforced by the calculation of the average cost where the difference in cost for different eigenstates is much larger than in the case of the ground state.

Chapter 6

Summary and Conclusions

In this thesis I have have investigated the advantages of incorporating supersymmetric quantum mechanics in the description of quantum control protocols. Using two different protocols, a quench and a shortcut to adiabaticity via counterdiabatic driving, I have developed a general description of the supersymmetric treatment of these protocols and how the intertwining properties of supersymmetry can be used to describe different processes.

My work resulted in two publications in peer-reviewed journals that are the basis for Chapters 4 and 5. These publications are embedded in the manuscript before the conclusions and final remarks of each section and I will briefly summarize the main results of each Chapter. For future directions specific to topic I ask the readers to please refer to the remarks section of each chapter.

6.1 Chapter 4: Non-equilibrium many-body dynamics in supersymmetric systems

In this work I used supersymmetric partner potentials in quenching protocols in order to study an out-of-equilibrium Fermi gases and observed the dynamics that follow post quench. In general by using supersymmetric partner potentials for the purposes of quenching, calculations such as the survival probability and work probability distribution can be simplified due to the degeneracy of the eigenspectra between potentials. This is accomplished by taking advantage of the intertwining properties between the Hamiltonians constructed using the factorization methods of supersymmetry. As a case example I have shown that for the infinite square well, this leads to interesting dynamics such as the preservation of quantum revivals at finite temperature. In this particular quench, the preservation of the n^2 eigenspectrum from the initial potential are the central cause of this phenomenon. This was carefully shown by studying the time dependent exponential term of the survival probability where at the times when all wavefunctions possess a phase factor of $0 \mod 2\pi$ a revival will occur. This refocusing of the phase, however, is not universal for supersymmetric quenches between arbitrary potentials and should be investigated on a case by case basis depending on the eigenspectra of the initial potential. As an example I presented a supersymmetric quench that also contains an n^2 dependence in its eigenspectrum however the revival

retention is doubled compared to the ISW partner potential quench. The main results highlighting the methods used for the ISW can be found at Phys. Rev. Research **4**, 033014 (2022) [1].

6.2 Chapter 5: Quantum control and quantum speed limits in supersymmetric potentials

In this work I incorporated supersymmetric quantum mechanics into STA protocols, most notably for counterdiabatic driving. This is motivated by the construction of the counterdiabatic driving term where in order to keep an eigenstate of a time-dependent Hamiltonian at perfect fidelity over time the instantaneous eigenstates and eigenspectra need to be known at all times. Using the ISW to test this concept, I have shown that by moving to higher order potentials, values such as the fidelity, cost of driving and QSL time improve. This is tested for two sets of wavefunctions over three neighbouring potentials, the ground state wavefunctions and three wavefunctions isospectral to one another. I have also presented a method in which the intertwining properties of supersymmetry can be incorporated into counterdiabatic driving. Starting with the construction of partner Hamiltonians via the factorization methods of supersymmetry, I have shown that the operators can be used to construct an intertwining property between isospectral counterdiabatic driving Hamiltonians. As a consequence of these extensions of the intertwining properties, relationships in values such as the cost of driving a system were presented. The main results of this work can be found at New J. Phys. **24**, 095001 (2022) [2].

Bibliography

[1] C. Campbell, T. Fogarty, and T. Busch, *Nonequilibrium many-body dynamics in supersymmetric quenching*, Phys. Rev. Research **4**, 033014 (2022).

[2] C. Campbell, J. Li, T. Busch, and T. Fogarty, *Quantum control and quantum speed limits in supersymmetric potentials*, New Journal of Physics **24**, 095001 (2022).

[3] I. Bloch, *Ultracold quantum gases in optical lattices*, Nature Physics **1**, 23–30 (2005).

[4] L. Amico, G. Birkl, M. Boshier, and L.-C. Kwek, *Focus on atomtronics-enabled quantum technologies*, New Journal of Physics **19**, 020201 (2017).

[5] A. Acín, I. Bloch, H. Buhrman, T. Calarco, C. Eichler, J. Eisert, D. Esteve, N. Gisin, S. J. Glaser, F. Jelezko, S. Kuhr, M. Lewenstein, M. F. Riedel, P. O. Schmidt, R. Thew, A. Wallraff, I. Walmsley, and F. K. Wilhelm, *The quantum technologies roadmap: a European community view*, New Journal of Physics **20**, 080201 (2018).

[6] L. Amico, M. Boshier, G. Birkl, A. Minguzzi, C. Miniatura, L.-C. Kwek, D. Aghamalyan, V. Ahufinger, D. Anderson, N. Andrei, A. S. Arnold, M. Baker, T. A. Bell, T. Bland, J. P. Brantut, D. Cassettari, W. J. Chetcuti, F. Chevy, R. Citro, S. De Palo, R. Dumke, M. Edwards, R. Folman, J. Fortagh, S. A. Gardiner, B. M. Garraway, G. Gauthier, A. Günther, T. Haug, C. Hufnagel, M. Keil, P. Ireland, M. Lebrat, W. Li, L. Longchambon, J. Mompart, O. Morsch, P. Naldesi, T. W. Neely, M. Olshanii, E. Orignac, S. Pandey, A. Pérez-Obiol, H. Perrin, L. Piroli, J. Polo, A. L. Pritchard, N. P. Proukakis, C. Rylands, H. Rubinsztein-Dunlop, F. Scazza, S. Stringari, F. Tosto, A. Trombettoni, N. Victorin, W. v. Klitzing, D. Wilkowski, K. Xhani, and A. Yakimenko, *Roadmap on Atomtronics: State of the art and perspective*, AVS Quantum Science **3**, 039201 (2021).

[7] D. Barredo, V. Lienhard, S. de Léséleuc, T. Lahaye, and A. Browaeys, *Synthetic three-dimensional atomic structures assembled atom by atom*, Nature **561**, 79–82 (2018).

[8] F. Cooper, A. Khare, and U. Sukhatme, *Supersymmetry and quantum mechanics*, Physics Reports **251**, 267–385 (1995).

[9] E. Schrödinger, *A Method of Determining Quantum-Mechanical Eigenvalues and Eigenfunctions*, Proceedings of the Royal Irish Academy. Section A: Mathematical and Physical Sciences **46**, 9–16 (1940).

[10] L. Infeld and T. E. Hull, *The Factorization Method*, Rev. Mod. Phys. **23**, 21–68 (1951).

[11] A. Andrianov, N. Borisov, and M. Ioffe, *The factorization method and quantum systems with equivalent energy spectra*, Physics Letters A **105**, 19–22 (1984).

[12] R. Dutt, A. Khare, and U. P. Sukhatme, *Supersymmetry, shape invariance, and exactly solvable potentials*, American Journal of Physics **56**, 163–168 (1988).

[13] F. Cooper, J. N. Ginocchio, and A. Wipf, *Supersymmetry, operator transformations and exactly solvable potentials*, Journal of Physics A: Mathematical and General **22**, 3707–3716 (1989).

[14] J. Benbourenane and H. Eleuch, *Exactly solvable new classes of potentials with finite discrete energies*, Results in Physics **17**, 103034 (2020).

[15] M. Tomka, M. Pletyukhov, and V. Gritsev, *Supersymmetry in quantum optics and in spin-orbit coupled systems*, Scientific Reports **5**, 13097 (2015).

[16] M. Lahrz, C. Weitenberg, and L. Mathey, *Implementing supersymmetric dynamics in ultracold-atom systems*, Phys. Rev. A **96**, 043624 (2017).

[17] X.-W. Luo, M. G. Raizen, and C. Zhang, *Supersymmetry-assisted high-fidelity ground-state preparation of a single neutral atom in an optical tweezer*, Phys. Rev. A **103**, 012415 (2021).

[18] J. Goold, T. Fogarty, N. Lo Gullo, M. Paternostro, and T. Busch, *Orthogonality catastrophe as a consequence of qubit embedding in an ultracold Fermi gas*, Phys. Rev. A **84**, 063632 (2011).

[19] S. Campbell, M. A. García-March, T. Fogarty, and T. Busch, *Quenching small quantum gases: Genesis of the orthogonality catastrophe*, Phys. Rev. A **90**, 013617 (2014).

[20] M. Á. García-March, T. Fogarty, S. Campbell, T. Busch, and M. Paternostro, *Non-equilibrium thermodynamics of harmonically trapped bosons*, New Journal of Physics **18**, 103035 (2016).

[21] A. Mostafazadeh, *Supersymmetric dynamical invariants*, Journal of Physics A: Mathematical and General **34**, 4493–4505 (2001).

[22] K. Zelaya and V. Hussin, *Time-dependent rational extensions of the parametric oscillator: quantum invariants and the factorization method*, Journal of Physics A: Mathematical and Theoretical **53**, 165301 (2020).

[23] M. H. Anderson, J. R. Ensher, M. R. Matthews, C. E. Wieman, and E. A. Cornell, *Observation of Bose-Einstein Condensation in a Dilute Atomic Vapor*, Science **269**, 198–201 (1995).

[24] K. B. Davis, M. O. Mewes, M. R. Andrews, N. J. van Druten, D. S. Durfee, D. M. Kurn, and W. Ketterle, *Bose-Einstein Condensation in a Gas of Sodium Atoms*, Phys. Rev. Lett. **75**, 3969–3973 (1995).

[25] E. L. Raab, M. Prentiss, A. Cable, S. Chu, and D. E. Pritchard, *Trapping of Neutral Sodium Atoms with Radiation Pressure*, Phys. Rev. Lett. **59**, 2631–2634 (1987).

[26] T. Hänsch and A. Schawlow, *Cooling of gases by laser radiation*, Optics Communications **13**, 68–69 (1975).

[27] D. J. Wineland, R. E. Drullinger, and F. L. Walls, *Radiation-Pressure Cooling of Bound Resonant Absorbers*, Phys. Rev. Lett. **40**, 1639–1642 (1978).

[28] C. E. Wieman, D. E. Pritchard, and D. J. Wineland, *Atom cooling, trapping, and quantum manipulation*, Rev. Mod. Phys. **71**, S253–S262 (1999).

[29] B. DeMarco and D. S. Jin, *Onset of Fermi Degeneracy in a Trapped Atomic Gas*, Science **285**, 1703–1706 (1999).

[30] F. Schreck, L. Khaykovich, K. L. Corwin, G. Ferrari, T. Bourdel, J. Cubizolles, and C. Salomon, *Quasipure Bose-Einstein Condensate Immersed in a Fermi Sea*, Phys. Rev. Lett. **87**, 080403 (2001).

[31] H. Friedrich, *Theoretical Atomic Physics*, Springer International Publishing (2017).

[32] D. Griffiths, *Introduction to Electrodynamics*, Pearson Education (2014).

[33] P. Windpassinger and K. Sengstock, *Engineering novel optical lattices*, Reports on Progress in Physics **76**, 086401 (2013).

[34] Y. Yang, Y. Ren, M. Chen, Y. Arita, and C. Rosales-Guzmán, *Optical trapping with structured light: a review*, Advanced Photonics **3**, 034001 (2021).

[35] P. Jessen and I. Deutsch. *Optical Lattices.* volume 37 of *Advances In Atomic, Molecular, and Optical Physics*, pages 95–138. Academic Press, (1996).

[36] I. Bloch, J. Dalibard, and W. Zwerger, *Many-body physics with ultracold gases*, Rev. Mod. Phys. **80**, 885–964 (2008).

[37] M. T. Batchelor, *Beautiful Models: 70 Years of Exactly Solved Quantum Many-Body Problems*, Journal of Physics A: Mathematical and General **38**, 3245–3246 (2005).

[38] B. Paredes, A. Widera, V. Murg, O. Mandel, S. Fölling, I. Cirac, G. V. Shlyapnikov, T. W. Hänsch, and I. Bloch, *Tonks–Girardeau gas of ultracold atoms in an optical lattice*, Nature **429**, 277–281 (2004).

[39] T. Kinoshita, T. Wenger, and D. S. Weiss, *Observation of a one-dimensional Tonks-Girardeau gas*, Science **305**, 1125–1128 (2004).

[40] A. G. Truscott, K. E. Strecker, W. I. McAlexander, G. B. Partridge, and R. G. Hulet, *Observation of Fermi Pressure in a Gas of Trapped Atoms*, Science **291**, 2570–2572 (2001).

[41] C. Chin, M. Bartenstein, A. Altmeyer, S. Riedl, S. Jochim, J. H. Denschlag, and R. Grimm, *Observation of the pairing gap in a strongly interacting Fermi gas*, Science **305**, 1128–1130 (2004).

[42] C. A. Regal, M. Greiner, and D. S. Jin, *Observation of Resonance Condensation of Fermionic Atom Pairs*, Phys. Rev. Lett. **92**, 040403 (2004).

[43] T. Bourdel, L. Khaykovich, J. Cubizolles, J. Zhang, F. Chevy, M. Teichmann, L. Tarruell, S. J. J. M. F. Kokkelmans, and C. Salomon, *Experimental Study of the BEC-BCS Crossover Region in Lithium 6*, Phys. Rev. Lett. **93**, 050401 (2004).

[44] S. Giorgini, L. P. Pitaevskii, and S. Stringari, *Theory of ultracold atomic Fermi gases*, Rev. Mod. Phys. **80**, 1215–1274 (2008).

[45] S. E. Olson, M. L. Terraciano, M. Bashkansky, and F. K. Fatemi, *Cold-atom confinement in an all-optical dark ring trap*, Phys. Rev. A **76**, 061404 (2007).

[46] L. Amico, A. Osterloh, and F. Cataliotti, *Quantum Many Particle Systems in Ring-Shaped Optical Lattices*, Phys. Rev. Lett. **95**, 063201 (2005).

[47] S. Franke-Arnold, J. Leach, M. J. Padgett, V. E. Lembessis, D. Ellinas, A. J. Wright, J. M. Girkin, P. Öhberg, and A. S. Arnold, *Optical ferris wheel for ultracold atoms*, Opt. Express **15**, 8619–8625 (2007).

[48] A. S. Arnold, *Extending dark optical trapping geometries*, Opt. Lett. **37**, 2505–2507 (2012).

[49] D. Barredo, S. de Léséleuc, V. Lienhard, T. Lahaye, and A. Browaeys, *An atom-by-atom assembler of defect-free arbitrary two-dimensional atomic arrays*, Science **354**, 1021–1023 (2016).

[50] H. Tamura, T. Unakami, J. He, Y. Miyamoto, and K. Nakagawa, *Highly uniform holographic microtrap arrays for single atom trapping using a feedback optimization of in-trap fluorescence measurements*, Opt. Express **24**, 8132–8141 (2016).

[51] M. Endres, H. Bernien, A. Keesling, H. Levine, E. R. Anschuetz, A. Krajenbrink, C. Senko, V. Vuletic, M. Greiner, and M. D. Lukin, *Atom-by-atom assembly of defect-free one-dimensional cold atom arrays*, Science **354**, 1024–1027 (2016).

[52] H. Rubinsztein-Dunlop, A. Forbes, M. V. Berry, M. R. Dennis, D. L. Andrews, M. Mansuripur, C. Denz, C. Alpmann, P. Banzer, T. Bauer, E. Karimi, L. Marrucci, M. Padgett, M. Ritsch-Marte, N. M. Litchinitser, N. P. Bigelow, C. Rosales-Guzmán, A. Belmonte, J. P. Torres, T. W. Neely, M. Baker, R. Gordon, A. B. Stilgoe, J. Romero, A. G. White, R. Fickler, A. E. Willner, G. Xie, B. McMorran, and A. M. Weiner, *Roadmap on structured light*, Journal of Optics **19**, 013001 (2016).

[53] L. Amico, D. Anderson, M. Boshier, J.-P. Brantut, L.-C. Kwek, A. Minguzzi, and W. von Klitzing, *Colloquium: Atomtronic circuits: From many-body physics to quantum technologies*, Rev. Mod. Phys. **94**, 041001 (2022).

[54] D. Cassettari, G. Mussardo, and A. Trombettoni. *Holographic Realization of the Prime Number Quantum Potential*, (2022).

[55] P. A. M. Dirac, *The Principles of Quantum Mechanics*, Clarendon Press (1930).

[56] L. Infeld, *On a New Treatment of Some Eigenvalue Problems*, Phys. Rev. **59**, 737–747 (1941).

[57] T. E. Hull and L. Infeld, *The Factorization Method, Hydrogen Intensities, and Related Problems*, Phys. Rev. **74**, 905–909 (1948).

[58] C. V. Sukumar, *Supersymmetry, factorisation of the Schrödinger equation and a Hamiltonian hierarchy*, Journal of Physics A: Mathematical and General **18**, L57–L61 (1985).

[59] R. Shankar, *Principles of quantum mechanics*, Kluwer Academic/Plenum, New York, NY, 2 edition (1994).

[60] K. Gutierrez, E. León, M. Belloni, and R. W. Robinett, *Exact results for the infinite supersymmetric extensions of the infinite square well*, European Journal of Physics **39**, 065404 (2018).

[61] M. Abramowitz and I. Stegun, *Handbook of Mathematical Functions: With Formulas, Graphs, and Mathematical Tables*, Dover Publications (1965).

[62] M. Danos, M. Abramowitz, J. Rafelski, and I. Stegun, *Pocketbook of Mathematical Functions*, H. Deutsch (1984).

[63] A. Contreras-Astorga and D. J. F. C, *Supersymmetric partners of the trigonometric Pöschl–Teller potentials*, Journal of Physics A: Mathematical and Theoretical **41**, 475303 (2008).

[64] J. V. Mallow, A. Gangopadhyaya, J. Bougie, and C. Rasinariu, *Inter-relations between additive shape invariant superpotentials*, Physics Letters A **384**, 126129 (2020).

[65] J. Lekner, *Reflectionless eigenstates of the sech2 potential*, American Journal of Physics **75**, 1151–1157 (2007).

[66] A. D. Alhaidari, *The supersymmetric Jaynes–Cummings model and its solutions*, Journal of Physics A: Mathematical and General **39**, 15391–15401 (2006).

[67] E. Cattaruzza, E. Gozzi, and C. Pagani, *Entanglement, superselection rules and supersymmetric quantum mechanics*, Physics Letters A **378**, 2501–2504 (2014).

[68] H. P. Laba and V. M. Tkachuk, *Entangled states in supersymmetric quantum mechanics*, Modern Physics Letters A **35**, 2050282 (2020).

[69] M. Heinrich, M.-A. Miri, R. El-Ganainy, and D. N. Christodoulides. *Selective mode filtering in supersymmetric optical structures*. In *Frontiers in Optics 2013*, page FTh2E.3. Optica Publishing Group, (2013).

[70] M.-A. Miri, M. Heinrich, R. El-Ganainy, and D. N. Christodoulides, *Supersymmetric Optical Structures*, Phys. Rev. Lett. **110**, 233902 (2013).

[71] M. Heinrich, M.-A. Miri, S. Stützer, R. El-Ganainy, S. Nolte, A. Szameit, and D. N. Christodoulides, *Supersymmetric mode converters*, Nature Communications **5**, 3698 (2014).

[72] G. Queraltó, V. Ahufinger, and J. Mompart, *Mode-division (de)multiplexing using adiabatic passage and supersymmetric waveguides*, Opt. Express **25**, 27396–27404 (2017).

[73] G. Queraltó, V. Ahufinger, and J. Mompart, *Integrated photonic devices based on adiabatic transitions between supersymmetric structures*, Opt. Express **26**, 33797–33806 (2018).

[74] K. Y. Bhagat, B. Bose, S. Choudhury, S. Chowdhury, R. N. Das, S. G. Dastider, N. Gupta, A. Maji, G. D. Pasquino, and S. Paul, *The Generalized OTOC from Supersymmetric Quantum Mechanics—Study of Random Fluctuations from Eigenstate Representation of Correlation Functions*, Symmetry **13** (2021).

[75] V. G. Bagrov and B. F. Samsonov, *Supersymmetry of a nonstationary Schrödinger equation*, Physics Letters A **210**, 60–64 (1996).

[76] D. J. Arrigo and F. Hickling, *An nth-order Darboux transformation for the one-dimensional time-dependent Schrödinger equation*, Journal of Physics A: Mathematical and General **36**, 1615–1621 (2003).

[77] D. Rasinskaitė and P. Strange, *Quantum surfing*, European Journal of Physics **42**, 015402 (2020).

[78] P. Strange, *Quantum potential in time-dependent supersymmetric quantum mechanics*, Phys. Rev. A **104**, 062213 (2021).

[79] C. Grossmann, H. Roos, and M. Stynes, *Numerical Treatment of Partial Differential Equations*, Springer Berlin Heidelberg (2007).

[80] J. Crank and P. Nicolson, *A practical method for numerical evaluation of solutions of partial differential equations of the heat-conduction type*, Mathematical Proceedings of the Cambridge Philosophical Society **43**, 50–67 (1947).

[81] B. Fornberg, *Generation of Finite Difference Formulas on Arbitrarily Spaced Grids*, Mathematics of Computation **51**, 699–706 (1988).

[82] A. Askar and A. S. Cakmak, *Explicit integration method for the time-dependent Schrödinger equation for collision problems*, The Journal of Chemical Physics **68**, 2794–2798 (1978).

[83] C. Leforestier, R. Bisseling, C. Cerjan, M. Feit, R. Friesner, A. Guldberg, A. Hammerich, G. Jolicard, W. Karrlein, H.-D. Meyer, N. Lipkin, O. Roncero, and R. Kosloff, *A comparison of different propagation schemes for the time dependent Schrödinger equation*, Journal of Computational Physics **94**, 59–80 (1991).

[84] W. Press, S. Teukolsky, W. Vetterling, and B. Flannery, *Numerical Recipes 3rd Edition: The Art of Scientific Computing*, Cambridge University Press (2007).

[85] A. Sindona, J. Goold, N. L. Gullo, and F. Plastina, *Statistics of the work distribution for a quenched Fermi gas*, New Journal of Physics **16**, 045013 (2014).

[86] J. Goold, F. Plastina, A. Gambassi, and A. Silva. *The Role of Quantum Work Statistics in Many-Body Physics*, pages 317–336. Springer International Publishing, Cham, (2018).

[87] M. Srednicki, *Chaos and quantum thermalization*, Phys. Rev. E **50**, 888–901 (1994).

[88] P. W. Anderson, *Infrared Catastrophe in Fermi Gases with Local Scattering Potentials*, Phys. Rev. Lett. **18**, 1049–1051 (1967).

[89] P. W. Anderson, *Absence of Diffusion in Certain Random Lattices*, Phys. Rev. **109**, 1492–1505 (1958).

[90] R. Abou-Chacra, D. J. Thouless, and P. W. Anderson, *A selfconsistent theory of localization*, Journal of Physics C: Solid State Physics **6**, 1734–1752 (1973).

[91] E. Abrahams, *50 Years of Anderson Localization*, WORLD SCIENTIFIC (2010).

[92] D. S. Hall, M. R. Matthews, J. R. Ensher, C. E. Wieman, and E. A. Cornell, *Dynamics of Component Separation in a Binary Mixture of Bose-Einstein Condensates*, Phys. Rev. Lett. **81**, 1539–1542 (1998).

[93] C. Kohstall, M. Zaccanti, M. Jag, A. Trenkwalder, P. Massignan, G. M. Bruun, F. Schreck, and R. Grimm, *Metastability and coherence of repulsive polarons in a strongly interacting Fermi mixture*, Nature **485**, 615–618 (2012).

[94] M. Cetina, M. Jag, R. S. Lous, I. Fritsche, J. T. M. Walraven, R. Grimm, J. Levinsen, M. M. Parish, R. Schmidt, M. Knap, and E. Demler, *Ultrafast many-body interferometry of impurities coupled to a Fermi sea*, Science **354**, 96–99 (2016).

[95] R. Schmidt, M. Knap, D. A. Ivanov, J.-S. You, M. Cetina, and E. Demler, *Universal many-body response of heavy impurities coupled to a Fermi sea: a review of recent progress*, Reports on Progress in Physics **81**, 024401 (2018).

[96] M. Mikkelsen, T. Fogarty, and T. Busch, *Connecting Scrambling and Work Statistics for Short-Range Interactions in the Harmonic Oscillator*, Phys. Rev. Lett. **128**, 070605 (2022).

[97] M. Á. García-March, T. Fogarty, S. Campbell, T. Busch, and M. Paternostro, *Non-equilibrium thermodynamics of harmonically trapped bosons*, New Journal of Physics **18**, 103035 (2016).

[98] A. S. Campbell, D. M. Gangardt, and K. V. Kheruntsyan, *Sudden Expansion of a One-Dimensional Bose Gas from Power-Law Traps*, Phys. Rev. Lett. **114**, 125302 (2015).

[99] W. Rohringer, D. Fischer, F. Steiner, I. E. Mazets, J. Schmiedmayer, and M. Trupke, *Non-equilibrium scale invariance and shortcuts to adiabaticity in a one-dimensional Bose gas*, Scientific Reports **5** (2015).

[100] E. Vogt, M. Feld, B. Fröhlich, D. Pertot, M. Koschorreck, and M. Köhl, *Scale Invariance and Viscosity of a Two-Dimensional Fermi Gas*, Phys. Rev. Lett. **108**, 070404 (2012).

[101] Y. Y. Atas, A. Safavi-Naini, and K. V. Kheruntsyan, *Nonequilibrium quantum thermodynamics of determinantal many-body systems: Application to the Tonks-Girardeau and ideal Fermi gases*, Phys. Rev. A **102**, 043312 (2020).

[102] R. Schmitz, S. Krönke, L. Cao, and P. Schmelcher, *Quantum breathing dynamics of ultracold bosons in one-dimensional harmonic traps: Unraveling the pathway from few- to many-body systems*, Phys. Rev. A **88**, 043601 (2013).

[103] B. Fang, G. Carleo, A. Johnson, and I. Bouchoule, *Quench-Induced Breathing Mode of One-Dimensional Bose Gases*, Phys. Rev. Lett. **113**, 035301 (2014).

[104] A. I. Gudyma, G. E. Astrakharchik, and M. B. Zvonarev, *Reentrant behavior of the breathing-mode-oscillation frequency in a one-dimensional Bose gas*, Phys. Rev. A **92**, 021601 (2015).

[105] M. Łebek, P. T. Grochowski, and K. Rzążewski, *Single- to many-body crossover of a quantum carpet*, Phys. Rev. Research **3**, 023009 (2021).

[106] H. T. E. F.R.S., *LXXVI. Facts relating to optical science. No. IV*, The London, Edinburgh, and Dublin Philosophical Magazine and Journal of Science **9**, 401–407 (1836).

[107] L. Deng, E. W. Hagley, J. Denschlag, J. E. Simsarian, M. Edwards, C. W. Clark, K. Helmerson, S. L. Rolston, and W. D. Phillips, *Temporal, Matter-Wave-Dispersion Talbot Effect*, Phys. Rev. Lett. **83**, 5407–5411 (1999).

[108] C. Kittel, H. Charles Kittel, K. Charles, H. Kroemer, and K. Herbert, *Thermal Physics*, W. H. Freeman (1980).

[109] C. Kittel, *Introduction to solid state physics*, John Wiley & Sons, Nashville, TN, 8 edition (2004).

[110] F. M. Cucchietti, H. M. Pastawski, and D. A. Wisniacki, *Decoherence as decay of the Loschmidt echo in a Lorentz gas*, Phys. Rev. E **65**, 045206 (2002).

[111] F. M. Cucchietti, D. A. R. Dalvit, J. P. Paz, and W. H. Zurek, *Decoherence and the Loschmidt Echo*, Phys. Rev. Lett. **91**, 210403 (2003).

[112] J. J. Loschmidt, *"Über den Zustand des Wärmegleichgewichts eines Systems von Körpern mit Rücksicht auf die Schwerkraft"*, Sitzungsberichte der Akademie der Wissenschaften **2**, 128–142 (1876).

[113] T. Gorin, T. Prosen, T. H. Seligman, and M. Žnidarič, *Dynamics of Loschmidt echoes and fidelity decay*, Physics Reports **435**, 33–156 (2006).

[114] M. Knap, A. Shashi, Y. Nishida, A. Imambekov, D. A. Abanin, and E. Demler, *Time-Dependent Impurity in Ultracold Fermions: Orthogonality Catastrophe and Beyond*, Phys. Rev. X **2**, 041020 (2012).

[115] M. Gebert, H. Küttler, and P. Müller, *Anderson's Orthogonality Catastrophe*, Communications in Mathematical Physics **329**, 979–998 (2014).

[116] A. del Campo, *Long-time behavior of many-particle quantum decay*, Phys. Rev. A **84**, 012113 (2011).

[117] L. Levitov and G. Lesovik, *Charge distribution in quantum shot noise*, Jetp Letters - JETP LETT-ENGL TR **58** (1993).

[118] I. Klich and Y. V. Nazarov. *An Elementary Derivation of Levitov's Formula*, pages 397–402. Springer Netherlands, Dordrecht, (2003).

[119] D. A. Abanin and L. S. Levitov, *Fermi-Edge Resonance and Tunneling in Nonequilibrium Electron Gas*, Phys. Rev. Lett. **94**, 186803 (2005).

[120] K. Schönhammer, *Full counting statistics for noninteracting fermions: Exact results and the Levitov-Lesovik formula*, Phys. Rev. B **75**, 205329 (2007).

[121] R. Schmidt, M. Knap, D. A. Ivanov, J.-S. You, M. Cetina, and E. Demler, *Universal many-body response of heavy impurities coupled to a Fermi sea: a review of recent progress*, Reports on Progress in Physics **81**, 024401 (2018).

[122] M. T. Mitchison, T. Fogarty, G. Guarnieri, S. Campbell, T. Busch, and J. Goold, *In Situ Thermometry of a Cold Fermi Gas via Dephasing Impurities*, Phys. Rev. Lett. **125**, 080402 (2020).

[123] L. Oghittu and A. Negretti, *Quantum-limited thermometry of a Fermi gas with a charged spin particle*, Phys. Rev. Research **4**, 023069 (2022).

[124] M. Esposito, U. Harbola, and S. Mukamel, *Nonequilibrium fluctuations, fluctuation theorems, and counting statistics in quantum systems*, Rev. Mod. Phys. **81**, 1665–1702 (2009).

[125] M. Campisi, P. Hänggi, and P. Talkner, *Colloquium: Quantum fluctuation relations: Foundations and applications*, Rev. Mod. Phys. **83**, 771–791 (2011).

[126] E. Vicari, *Particle-number scaling of the quantum work statistics and Loschmidt echo in Fermi gases with time-dependent traps*, Phys. Rev. A **99**, 043603 (2019).

[127] P. Talkner, E. Lutz, and P. Hänggi, *Fluctuation theorems: Work is not an observable*, Phys. Rev. E **75**, 050102 (2007).

[128] T. Dowdall, A. Benseny, T. Busch, and A. Ruschhaupt, *Fast and robust quantum control based on Pauli blocking*, Phys. Rev. A **96**, 043601 (2017).

[129] T. K. Timberlake and S. Camp, *Decay of wave packet revivals in the asymmetric infinite square well*, American Journal of Physics **79**, 607–614 (2011).

[130] P. T. Grochowski, T. Karpiuk, M. Brewczyk, and K. Rzążewski, *Fermionic quantum carpets: From canals and ridges to solitonlike structures*, Phys. Rev. Research **2**, 013119 (2020).

[131] A. S. Sanz and S. Miret-Artés, *A causal look into the quantum Talbot effect*, The Journal of Chemical Physics **126**, 234106 (2007).

[132] A. Bakman, S. Fishman, M. Fink, E. Fort, and S. Wildeman, *Observation of the Talbot effect with water waves*, American Journal of Physics **87**, 38–43 (2019).

[133] L. A. Hall, M. Yessenov, S. A. Ponomarenko, and A. F. Abouraddy, *The space–time Talbot effect*, APL Photonics **6**, 056105 (2021).

[134] F. Saif, *Talbot effect with matter waves*, Laser Physics **22**, 1874–1878 (2012).

[135] F. Großmann, J.-M. Rost, and W. P. Schleich, *Spacetime structures in simple quantum systems*, Journal of Physics A: Mathematical and General **30**, L277–L283 (1997).

[136] P. Kazemi, S. Chaturvedi, I. Marzoli, R. F. O'Connell, and W. P. Schleich, *Quantum carpets: a tool to observe decoherence*, New Journal of Physics **15**, 013052 (2013).

[137] J. Parker and C. R. Stroud, *Coherence and decay of Rydberg wave Packets*, Phys. Rev. Lett. **56**, 716–719 (1986).

[138] R. Bluhm and V. A. Kostelecký, *Quantum defects and the long-term behavior of radial Rydberg wave packets*, Phys. Rev. A **50**, R4445–R4448 (1994).

[139] R. Bluhm, V. A. Kostelecký, and J. A. Porter, *The evolution and revival structure of localized quantum wave packets*, American Journal of Physics **64**, 944–953 (1996).

[140] D. L. Aronstein and C. R. Stroud, *Fractional wave-function revivals in the infinite square well*, Phys. Rev. A **55**, 4526–4537 (1997).

[141] R. W. Robinett, *Visualizing the collapse and revival of wave packets in the infinite square well using expectation values*, American Journal of Physics **68**, 410–420 (2000).

[142] D. F. Styer, *Quantum revivals versus classical periodicity in the infinite square well*, American Journal of Physics **69**, 56–62 (2001).

[143] R. Robinett, *Quantum wave packet revivals*, Physics Reports **392**, 1–119 (2004).

[144] M. Nauenberg, *Autocorrelation function and quantum recurrence of wavepackets*, Journal of Physics B: Atomic, Molecular and Optical Physics **23**, L385–L390 (1990).

[145] U. P. Sukhatme, *WKB Energy Levels for a Class of One-Dimensional Potentials*, American Journal of Physics **41**, 1015–1016 (1973).

[146] R. W. Robinett, *Wave packet revivals and quasirevivals in one-dimensional power law potentials*, Journal of Mathematical Physics **41**, 1801–1813 (2000).

[147] C. Cohen-Tannoudji, B. Diu, and F. Laloe, *Quantum mechanics, volume 2*, Wiley-VCH Verlag, Weinheim, Germany, 2 edition (2019).

[148] C. Leichtle, I. S. Averbukh, and W. P. Schleich, *Generic Structure of Multilevel Quantum Beats*, Phys. Rev. Lett. **77**, 3999–4002 (1996).

[149] C. Leichtle, I. S. Averbukh, and W. P. Schleich, *Multilevel quantum beats: An analytical approach*, Phys. Rev. A **54**, 5299–5312 (1996).

[150] E. Brown and L. Hernández de la Peña, *A Simplified Pöschl–Teller Potential: An Instructive Exercise for Introductory Quantum Mechanics*, Journal of Chemical Education **95**, 1989–1995 (2018).

[151] R. Jozsa, *Fidelity for Mixed Quantum States*, Journal of Modern Optics **41**, 2315–2323 (1994).

[152] E. Torrontegui, S. Ibáñez, X. Chen, A. Ruschhaupt, D. Guéry-Odelin, and J. G. Muga, *Fast atomic transport without vibrational heating*, Phys. Rev. A **83**, 013415 (2011).

[153] E. Torrontegui, X. Chen, M. Modugno, S. Schmidt, A. Ruschhaupt, and J. G. Muga, *Fast transport of Bose–Einstein condensates*, New Journal of Physics **14**, 013031 (2012).

[154] E. Torrontegui, X. Chen, M. Modugno, A. Ruschhaupt, D. Guéry-Odelin, and J. G. Muga, *Fast transitionless expansion of cold atoms in optical Gaussian-beam traps*, Phys. Rev. A **85**, 033605 (2012).

[155] J. Li, T. Fogarty, S. Campbell, X. Chen, and T. Busch, *An efficient nonlinear Feshbach engine*, New Journal of Physics **20**, 015005 (2018).

[156] Y.-Y. Chen, G. Watanabe, Y.-C. Yu, X.-W. Guan, and A. del Campo, *An interaction-driven many-particle quantum heat engine and its universal behavior*, npj Quantum Information **5**, 88 (2019).

[157] T. Keller, T. Fogarty, J. Li, and T. Busch, *Feshbach engine in the Thomas-Fermi regime*, Phys. Rev. Research **2**, 033335 (2020).

[158] M. Born and V. Fock, *Beweis des Adiabatensatzes*, Zeitschrift für Physik **51**, 165–180 (1928).

[159] T. Kato, *On the Adiabatic Theorem of Quantum Mechanics*, Journal of the Physical Society of Japan **5**, 435–439 (1950).

[160] M. Demirplak and S. A. Rice, *Adiabatic Population Transfer with Control Fields*, The Journal of Physical Chemistry A **107**, 9937–9945 (2003).

[161] M. V. Berry, *Transitionless quantum driving*, Journal of Physics A: Mathematical and Theoretical **42**, 365303 (2009).

[162] X. Chen, A. Ruschhaupt, S. Schmidt, A. del Campo, D. Guéry-Odelin, and J. G. Muga, *Fast Optimal Frictionless Atom Cooling in Harmonic Traps: Shortcut to Adiabaticity*, Phys. Rev. Lett. **104**, 063002 (2010).

[163] S. Deffner, C. Jarzynski, and A. del Campo, *Classical and Quantum Shortcuts to Adiabaticity for Scale-Invariant Driving*, Phys. Rev. X **4**, 021013 (2014).

[164] J. Deng, Q.-h. Wang, Z. Liu, P. Hänggi, and J. Gong, *Boosting work characteristics and overall heat-engine performance via shortcuts to adiabaticity: Quantum and classical systems*, Phys. Rev. E **88**, 062122 (2013).

[165] Y. Zheng and D. Poletti, *Quantum statistics and the performance of engine cycles*, Phys. Rev. E **92**, 012110 (2015).

[166] M. Beau, J. Jaramillo, and A. Del Campo, *Scaling-Up Quantum Heat Engines Efficiently via Shortcuts to Adiabaticity*, Entropy **18** (2016).

[167] S. Campbell and S. Deffner, *Trade-Off Between Speed and Cost in Shortcuts to Adiabaticity*, Phys. Rev. Lett. **118**, 100601 (2017).

[168] L. Mandelstam and I. Tamm. *The Uncertainty Relation Between Energy and Time in Non-relativistic Quantum Mechanics*, pages 115–123. Springer Berlin Heidelberg, Berlin, Heidelberg, (1991).

[169] N. Margolus and L. B. Levitin, *The maximum speed of dynamical evolution*, Physica D: Nonlinear Phenomena **120**, 188–195 (1998).

[170] L. B. Levitin and T. Toffoli, *Fundamental Limit on the Rate of Quantum Dynamics: The Unified Bound Is Tight*, Phys. Rev. Lett. **103**, 160502 (2009).

[171] S. Deffner and S. Campbell, *Quantum speed limits: from Heisenberg's uncertainty principle to optimal quantum control*, Journal of Physics A: Mathematical and Theoretical **50**, 453001 (2017).

[172] S. Deffner and E. Lutz, *Quantum Speed Limit for Non-Markovian Dynamics*, Phys. Rev. Lett. **111**, 010402 (2013).

[173] M. Demirplak and S. A. Rice, *Assisted Adiabatic Passage Revisited*, The Journal of Physical Chemistry B **109**, 6838–6844 (2005).

[174] A. del Campo, *Shortcuts to Adiabaticity by Counterdiabatic Driving*, Phys. Rev. Lett. **111**, 100502 (2013).

[175] C. Jarzynski, *Generating shortcuts to adiabaticity in quantum and classical dynamics*, Phys. Rev. A **88**, 040101 (2013).

[176] C. Jarzynski, *Geometric Phases and Anholonomy for a Class of Chaotic Classical Systems*, Phys. Rev. Lett. **74**, 1732–1735 (1995).

[177] A. d. Campo and M. G. Boshier, *Shortcuts to adiabaticity in a time-dependent box*, Scientific Reports **2**, 648 (2012).

[178] X. Chen, E. Torrontegui, D. Stefanatos, J.-S. Li, and J. G. Muga, *Optimal trajectories for efficient atomic transport without final excitation*, Phys. Rev. A **84**, 043415 (2011).

[179] D. Kirk, *Optimal Control Theory: An Introduction*, Dover Publications (2012).

[180] Y. Zheng, S. Campbell, G. De Chiara, and D. Poletti, *Cost of counterdiabatic driving and work output*, Phys. Rev. A **94**, 042132 (2016).

[181] V. M. Pérez-García, H. Michinel, J. I. Cirac, M. Lewenstein, and P. Zoller, *Low Energy Excitations of a Bose-Einstein Condensate: A Time-Dependent Variational Analysis*, Phys. Rev. Lett. **77**, 5320–5323 (1996).

[182] F. K. Abdullaev, J. G. Caputo, R. A. Kraenkel, and B. A. Malomed, *Controlling collapse in Bose-Einstein condensates by temporal modulation of the scattering length*, Phys. Rev. A **67**, 013605 (2003).

[183] T. Fogarty, L. Ruks, J. Li, and T. Busch, *Fast control of interactions in an ultracold two atom system: Managing correlations and irreversibility*, SciPost Phys. **6**, 021 (2019).

[184] Q. Zhang, X. Chen, and D. Guéry-Odelin, *Connection between Inverse Engineering and Optimal Control in Shortcuts to Adiabaticity*, Entropy **23** (2021).